J. Mater. Chem. A

ARTICLE

Cite this: DOI: 10.1039/x0xx00000x

Received 00th January 2012,
Accepted 00th January 2012

DOI: 10.1039/x0xx00000x

www.rsc.org/

Exploring simple ancillary ligands in copper-based dye-sensitized solar cells: effects of a heteroatom switch and of co-sensitization

Frederik J. Malzner,[a] Alessandro Prescimone,[a] Edwin C. Constable,[a] Catherine E. Housecroft*[a] and Markus Willgert[a]

The copper(I) complexes $[Cu(\mathbf{1})_2][PF_6]$, $[Cu(\mathbf{2})_2][PF_6]$, $[Cu(\mathbf{3})_2][PF_6]$ and $[Cu(\mathbf{4})_2][PF_6]$ (**1** = 2-(1H-imidazol-2-yl)-6-methylpyridine, **2** = 2-(6-methylpyridin-2-yl)oxazole, **3** = 2-(6-methylpyridin-2-yl)thiazole and **4** = 2-methyl-6-(1-methyl-1H-imidazol-2-yl)pyridine) are reported. The crystal structures of $[Cu(\mathbf{2})_2][PF_6]\cdot 0.5CH_2Cl_2$ and $[Cu(\mathbf{3})_2][PF_6]$ confirm *N,N'*-chelation modes for **2** and **3**, and tetrahedral copper(I). In the solution absorption spectra, the MLCT band shifts to lower energy with a change in heteroatom (O, 424 nm; NH, 435 nm; NMe, 446 nm; S, 465 nm). $[Cu(\mathbf{1})_2][PF_6]$ and $[Cu(\mathbf{4})_2][PF_6]$ undergo copper-centred oxidative processes at lower potential than the complexes with O or S heteroatoms. Heteroleptic complexes $[Cu(\mathbf{5})(L)]^+$ (**5** = ((6,6'-dimethyl-[2,2'-bipyridine]-4,4'-diyl)bis(4,1-phenylene))bis(phosphonic acid)), L = **1**–**4**) were assembled on FTO/TiO_2 electrodes. The shift in the MLCT band (O ~ NH < NMe < S) in the solid-state absorption spectra of the dye-functionalized electrodes parallels that of solution. The photoconversion efficiences (η) of masked, dye-sensitized solar cells (DSCs) containing $[Cu(\mathbf{5})(L)]^+$ (L = **1**–**4**) dyes and an I^-/I_3^- redox shuttle follow the order $[Cu(\mathbf{5})(\mathbf{1})]^+$ (3.03%) > $[Cu(\mathbf{5})(\mathbf{3})]^+$ (2.88%) > $[Cu(\mathbf{5})(\mathbf{4})]^+$ (2.71%) > $[Cu(\mathbf{5})(\mathbf{2})]^+$ (2.62%) relative to 7.55% for N719. Ancillary ligand **1** (with NH) leads to the highest open-circuit voltage (V_{OC} = 608 mV) whilst **3** (S-heteroatom) gives the highest short-circuit current density (J_{SC} = 7.76 mA cm^{-2}). The performances of $[Cu(\mathbf{5})(\mathbf{1})]^+$ and $[Cu(\mathbf{5})(\mathbf{3})]^+$ are understood with the aid of electrochemical impedance spectroscopy (EIS). The DSC with $[Cu(\mathbf{5})(\mathbf{1})]^+$ exhibits a high chemical capacitance (C_μ) and a low recombination resistance (R_{rec}); since the latter is offset by a low transport resistance (R_{tr}), a high J_{SC} and V_{OC} are observed for $[Cu(\mathbf{5})(\mathbf{1})]^+$. DSCs with $[Cu(\mathbf{5})(\mathbf{3})]^+$ have the lowest R_{tr} of all four devices. The performance of DSCs sensitized by a combination of $[Cu(\mathbf{5})(\mathbf{1})]^+$ and $[Cu(\mathbf{5})(\mathbf{3})]^+$ were assessed in order to capitalize upon the high V_{OC} of $[Cu(\mathbf{5})(\mathbf{1})]^+$ and the high J_{SC} of $[Cu(\mathbf{5})(\mathbf{3})]^+$. After FTO/$TiO_2$ functionalization with anchor **5**, the electrodes were treated with a 1:1 mix of $[Cu(\mathbf{5})(\mathbf{1})]^+$ and $[Cu(\mathbf{5})(\mathbf{3})]^+$ or sequentially with $[Cu(\mathbf{5})(\mathbf{3})]^+$ then $[Cu(\mathbf{5})(\mathbf{1})]^+$, or $[Cu(\mathbf{5})(\mathbf{1})]^+$ then $[Cu(\mathbf{5})(\mathbf{3})]^+$. The DSC performances and the EIS parameters are consistent with competition between **1** and **3** for surface binding-sites; **1** dominates over **3**, both in binding and in contribution to the overall photoresponse.

Introduction

The Grätzel n-type dye-sensitized solar cell (DSC)[1,2,3] converts solar photons into electrical energy. Conversion efficiencies of ~11–14% have been attained with state-of-the-art ruthenium-based, organic or zinc(II) porphyrin-based sensitizers.[4,5,6,7,8,9,10,11,12,13,14,15,16] Key factors in the development of DSCs are the improved design of 'push–pull' dyes, tuning of redox couples and compositions of liquid electrolytes, and the use of co-adsorbants and co-sensitizers. The fabrication of both the working and counter electrodes is also of crucial importance.[17] Ideally, a sensitizer in a DSC should be panchromatic, but in practice, many dyes have a limited absorption range. To overcome this, a second dye can be absorbed on the semiconductor surface to enhance the absorption spectrum in the regions where the first dye has only low spectral response. Further advantages of co-sensitization are a reduction in charge recombination, extended electron lifetime and a decrease in the total resistance of the DSC.[18] Because of their readily tuned and large absorption maxima, organic dyes are often the co-sensitizers of choice to complement ruthenium-based dyes;[19] intensely absorbing near-infrared dyes[20] and dyes that absorb between 300 and 500 nm[21] have attracted particular attention. Co-sensitization using zinc(II) porphyrins and organic dyes has led to notable enhancements of DSC performances,[22,23] and has enabled one of the highest power conversion efficiencies, η, of 12.3%.[24] Fan *et al.*[23] demonstrated that stepwise co-sensitization of a TiO_2

electrode with zinc(II) porphyrin-based and organic dyes rather than immersion of the electrode in a solution containing a mixture of these dyes led to improved DSC performance; sequential surface treatment with the zinc(II) porphyrin dye followed by organic sensitizer leads to better DSC performance than the opposite order.[23] Efficient panchromatic performance has also been achieved with a combination of a zinc(II) carboxyphthalocyanine and an organic co-sensitizer, although co-sensitization with phthalocyaninies does not routinely enhance DSC performance.[25] Co-sensitization using complementary organic dyes has received significant attention;[26] the combined effects of broadened absorption ranges (with respect to a single dye) leading to higher short-circuit current density (J_{SC}), and reduced charge recombination giving improved open-circuit voltages (V_{OC}) result in considerably enhanced photoconversion efficiencies.

Of particular relevance to our present investigation is co-sensitization using complementary inorganic dyes. Ranasinghe *et al.*[27] have investigated the co-sensitization with N719 and the ruthenium 'black dye' in solid-state DSCs, and demonstrated that the combination with the black dye increases light-harvesting close to 500 nm with respect to surfaces sensitized with N719 alone. Functionalization by dipping in a 1:1 cocktail of the two dyes improves both J_{SC} and V_{OC}, with increases in η from 3.8 or 3.0%, respectively, for N719 and the black dye individually, to 4.6% for the melange. It is proposed that the N719 helps to prevent aggregation of black dye on the TiO_2 surface.

Our interests in developing dyes for DSCs based on sustainable components focus on copper(I)-containing photosensitizers.[28] Within a relatively short timeframe, this area has witnessed milestone achievements, with photoconversion efficiencies reaching 4.66%.[28,29,30] Although strategic dye design predicates a 'push–pull' arrangement of ancillary ($L_{ancillary}$) and anchoring ligands (L_{anchor}), we have found that simple ancillary ligands combined with phosphonic acid anchoring ligands result in surprisingly good performances.[31,32] In most of our investigations, $L_{ancillary}$ has been based on a 6,6'-dimethyl-2,2'-bipyridine (dmbpy) scaffold, the methyl substituents preventing flattening of the copper(I) complex in the excited state. The steric bulk of the 6,6'-substituents effectively stabilizes copper(I) with respect to oxidation to copper(II).[33] We now present an investigation of four new copper(I)-based sensitizers which retain the N^N metal-binding domain of a diimine ligand in $L_{ancillary}$, but replace one pyridine ring of bpy by a 2-(1,3-benzoxazolyl), 2-benzimidazolyl or 2-(1,3-benzothiazolyl) unit. Differences in dye performances lead us to investigate co-sensitization strategies utilising two of these dyes which, when used alone exhibit, respectively, a high J_{SC} or a high V_{OC}.

Experimental

General. ^{1}H and ^{13}C NMR spectra were recorded on a Bruker Avance III-500 NMR spectrometer at 295 K unless otherwise stated; ^{1}H and ^{13}C chemical shifts were referenced to residual solvent peaks with respect to δ(TMS) = 0 ppm. Solution and solid state absorption spectra were recorded on an Agilent Cary 5000 UV-Vis-NIR spectrophotometer. Electrospray ionization (ESI) mass spectra were recorded on a Bruker Daltonics Inc. microflex instrument.

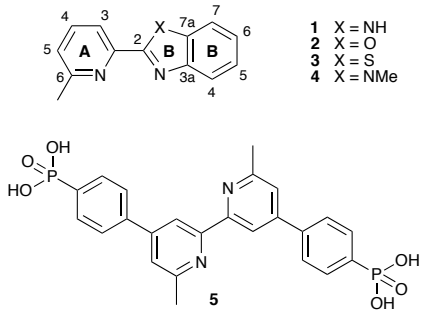

Scheme 1. Structures of the ancillary and anchoring ligands used in this study.

Electrochemical measurements were made using a CH Instruments 900B potentiostat with glassy carbon, platinum wire and and a leakless $AgCl/Ag^+$ electrode (eDAQ ET069) as the working, counter and reference electrodes, respectively. Samples were dissolved in dry CH_2Cl_2 (10^{-4} to 10^{-5} mol dm^{-3}) containing [^{n}Bu$_4$N][PF_6] (0.1 mol dm^{-3}) as the supporting electrolyte; all solutions were degassed with argon. Ferrocene was used as the internal reference.

Ligands **1**-**4** were prepared as previously described and NMR spectroscopic data matched those reported.[34,35,36,37,38,39] [Cu(MeCN)$_4$][PF_6] was prepared as reported.[40]

[Cu(1)$_2$][PF$_6$]. Ligand **1** (100 mg, 0.478 mmol) and [Cu(MeCN)$_4$][PF_6] (89.1 mg, 0.239 mmol) were stirred in MeCN (5 mL) under N_2. After 20 min the reaction mixture was filtered using a syringe filter and the solvent was removed over a warm-water bath under an N_2 stream. [Cu(**1**)$_2$][PF_6] was isolated as a red solid (147 mg, 0.234 mmol, 97.9%). The product is air-sensitive and should be stored under argon. ^{1}H NMR (500 MHz, acetone-d_6, 225 K, see text) δ / ppm 13.45 (s, 1H, H^{NH}), 8.26 (d, J = 8.0 Hz, 1H, H^{A3}), 8.13 (t, J = 7.7 Hz, 1H, H^{A4}), 7.70 (d, J = 8.0 Hz, 1H, H$^{B4/B7}$), 7.57 (d, J = 7.5 Hz, 1H, H^{A5}), 7.48 (d, J = 8.1 Hz, 1H, H$^{B4/B7}$), 7.35 (t, J = 7.5 Hz, 1H, H$^{B5/B6}$), 7.20 (t, J = 7.7 Hz, 1H, H$^{B5/B6}$), 2.12 (s, 3H, H^{Me}). ^{13}C NMR (126 MHz, acetone-d_6, 225 K) δ / ppm 139.8 (C^{A4}), 127.3 (C^{A5}), 126.0 (C$^{B5/B6}$), 124.5 (C$^{B5/B6}$), 119.6 (C^{A3}), 119.3 (C$^{B4/B7}$), 113.5 (C$^{B4/B7}$), 24.3 (C^{Me}). UV-Vis (CH_2Cl_2, 1.0 × 10^{-5} mol dm^{-3}): λ/nm (ε/dm^3 mol^{-1} cm^{-1}) 280 (sh, 14400), 312 (30000), 328 (29950), 435 (2980). ESI-MS *m/z* positive mode 481.1 [M–PF_6]$^+$ (calc. 481.1), negative mode 144.7 [PF_6]$^-$ (calc. 145.0). HR ESI-MS *m/z* positive mode 481.1198 [M–PF_6]$^+$ (calc. 481.1196). Satisfactory elemental analysis could not be obtained.

[Cu(2)$_2$][PF$_6$]. Ligand **2** (100 mg, 0.476 mmol) and [Cu(MeCN)$_4$][PF_6] (88.7 mg, 0.238 mmol) were stirred in MeCN (20 mL) for 20 min. The reaction mixture was filtered and the solvent was removed under reduced pressure. [Cu(**2**)$_2$][PF_6] was isolated as a red solid (150 mg, 0.238 mmol, 100%). ^{1}H NMR (500 MHz, CD_3CN) δ / ppm 8.18 (d, J = 7.6

Hz, 1H, H^{A3}), 7.97 (m, 1H, H^{A4}), 7.82 (d, J = 8.3 Hz, 1H, H^{B7}), 7.79 (d, J = 9.3 Hz, 1H, H^{B4}), 7.55 (d, J = 7.6 Hz, 1H, H^{A5}), 7.53 (ddd, J = 7.8, 7.6, 1.0 Hz, 1H, H^{B5}), 7.47 (ddd, J = 7.7, 7.5, 1.0 Hz, 1H, H^{B6}), 2.66 (s, 3H, H^{Me}). ^{13}C NMR (126 MHz, CD_3CN) δ / ppm 161.5 (C^{B2}), 160.3 (C^{A6}), 152.3 (C^{B3a}), 144.7 (C^{A2}), 141.1 (C^{B7a}), 139.3 (C^{A4}), 127.7 (C^{A5}), 127.6 (C^{B5}), 126.5 (C^{B6}), 121.6 (C^{A3}), 120.9 (C^{B7}), 112.4 (C^{B4}), 24.7 (C^{Me}). UV-Vis (CH_2Cl_2, 1.0 × 10^{-5} mol dm^{-3}): λ/nm (ε/dm^3 mol^{-1} cm^{-1}) 280 (sh, 23550), 299 (sh, 36800), 310 (45700), 323 (40100), 424 (4600). ESI-MS *m/z* positive mode 483.1 $[M–PF_6]^+$ (calc. 483.1); negative mode 144.9 $[PF_6]^-$ (calc. 145.0). Found: C 50.03, H 3.63, N 9.22; $C_{26}H_{20}CuF_6N_4O_2P$ requires C 49.65, H 3.21, N 8.91%.

[Cu(3)$_2$][PF$_6$]. The method was as for [Cu(**2**)$_2$][PF$_6$] starting with **3** (50.0 mg, 0.221 mmol) and [Cu(MeCN)$_4$][PF$_6$] (41.0 mg, 0.110 mmol). [Cu(**3**)$_2$][PF$_6$] was isolated as a red solid (72.7 mg, 0.110 mmol, 100%). ^{1}H NMR (500 MHz, CD_3CN) δ / ppm 8.10 (d, J = 7.7 Hz, 1H, H^{A3}), 8.09 (d, J = 7.5 Hz, 1H, H^{B7}), 8.06 (d, J = 8.2 Hz, 1H, H^{B4}), 7.94 – 7.88 (m, 1H, H^{A4}), 7.58 (ddd, J = 8.2, 7.0, 1.2 Hz, 1H, H^{B5}), 7.52 (ddd, J = 8.1, 7.1, 1.1 Hz, 1H, H^{B6}), 7.47 (d, J = 7.7 Hz, 1H, H^{A5}), 2.64 (s, 3H, H^{Me}). ^{13}C NMR (126 MHz, CD_3CN) δ 169.8 (C^{B2}), 160.0 (C^{A6}), 153.8 (C^{B3a}), 150.3 (C^{A2}), 139.2 (C^{A4}), 136.5 (C^{B7a}), 127.9 (C^{B5}), 127.3 (C^{B6}), 127.2 (C^{A5}), 124.0 (C^{B4}), 123.5 (C^{B7}), 119.8 (C^{A3}), 24.6 (C^{Me}). UV-Vis (CH_2Cl_2, 1.0 × 10^{-5} mol dm^{-3}): λ/nm (ε/dm^3 mol^{-1} cm^{-1}) 262 (21400), 284 (18400), 313 (sh, 34000), 329 (37500), 465 (5600). ESI-MS *m/z* positive mode 515.1 $[M–PF_6]^+$ (calc. 515.1); negative mode 144.6 $[PF_6]^-$ (calc. 145.0). HR-ESI MS *m/z* positive mode 515.0429 $[M–PF_6]^+$ (calc. 515.0420). Satisfactory elementary analysis could not be obtained.

[Cu(4)$_2$][PF$_6$]. The method was as for [Cu(**2**)$_2$][PF$_6$] starting with **4** (500 mg, 2.24 mmol) and [Cu(MeCN)$_4$][PF$_6$] (417 mg, 1.12 mmol). [Cu(**4**)$_2$][PF$_6$] was isolated as a red solid (691 mg, 1.06 mmol, 94.6%). ^{1}H NMR (500 MHz, CD_3CN) δ / ppm 8.07–8.03 (m, 1H, H^{A4}), 7.94 -7.90 (m, 2H, $H^{B4/B7}$), 7.79-7.76 (m, 2H, $H^{B5/B6}$), 7.74 (d, J = 7.8 Hz, 1H, H^{A3}), 7.64 (d, J = 7.9 Hz, 1H, H^{A5}), 4.01 (s, 3H, H^{NMe}), 2.68 (s, 3H, H^{Me}). ^{13}C NMR (126 MHz, CD_3CN) δ / ppm 161.8 (C^{A6}), 148.6 (C^{B2}), 141.0 (C^{A2}), 139.1 (C^{A4}), 133.0 (C^{B7a}), 128.2 ($C^{B5/B6}$), 127.9 (C^{A5}), 126.2 (C^{A3}), 114.1 ($C^{B4/B7}$), 32.8 (C^{NMe}), 24.4 (C^{Me}). UV-Vis (CH_2Cl_2, 1.0 × 10^{-5} mol dm^{-3}): λ/nm (ε/dm^3 mol^{-1} cm^{-1}) 282 (sh, 15200), 315 (27800), 328 (sh, 27000), 446 (2200). ESI-MS *m/z* positive mode 509.1 $[M–PF_6]^+$ (calc. 509.1); negative mode 144.9 $[PF_6]^-$ (calc. 145.0). HR-ESI MS *m/z* positive mode 509.1516 $[M–PF_6]^+$ (calc. 509.1509).

Crystallography. Single crystal data were collected on a Bruker APEX-II diffractometer; data reduction, solution and refinement used APEX2, SuperFlip and CRYSTALS respectively.[41,42,43] For [Cu(**2**)$_2$][PF$_6$]·0.5CH_2Cl_2, SQUEEZE[44] was used to treat the solvent region and the electron density removed equated to 0.5 CH_2Cl_2 per formula unit. Structure analysis used the program Mercury v. 3.6.[45,46]

[Cu(2)$_2$][PF$_6$]·0.5CH_2Cl_2. $C_{26.50}H_{21}ClCuF_6N_4O_2P$, M = 671.44, orange block, monoclinic, space group $C2/c$, a = 29.0226(18), b = 14.9554(10), c = 12.9437(9) Å, β = 90.929(4)°, U = 5617.4(6) Å^3, Z = 8, D_c = 1.59 Mg m^{-3}, μ(Cu-Kα) = 3.172 mm^{-1}, T = 123 K. Total 19041 reflections, 5039 unique, R_{int} = 0.030. Refinement of 4013 reflections (361 parameters) with I >2σ (I) converged at final R_1 = 0.1000 (R_1 all data = 0.1171), wR_2 = 0.2272 (wR_2 all data = 0.2359), gof = 1.0095. CCDC 1497681.

[Cu(3)$_2$][PF$_6$]. $C_{26}H_{20}CuF_6N_4PS_2$, M = 661.11, orange block, monoclinic, space group $P2_1/c$, a = 8.1188(3), b = 13.8910(5), c = 23.9522(9) Å, β = 92.0462(17)°, U = 2699.57(17) Å^3, Z = 4, D_c = 1.627 Mg m^{-3}, μ(Cu-Kα) = 3.752 mm^{-1}, T = 123 K. Total 34879 reflections, 4984 unique, R_{int} = 0.027. Refinement of 4925 reflections (361 parameters) with I >2σ (I) converged at final R_1 = 0.0883 (R_1 all data = 0.0888), wR_2 = 0.2242 (wR_2 all data = 0.2243), gof = 0.9825. CCDC 1497682.

Electrodes for solid-state absorption spectroscopy. Dye-functionalized electrodes were assembled as detailed below but using Solaronix Test Cell Titania Electrodes Transparent.

DSC fabrication and measurements. Solaronix Test Cell Titania Electrodes were washed with EtOH (HPLC grade), sintered at 450 °C (30 min), then cooled to ≈80 °C before being immersed in a solution of anchor **5** (DMSO, 1.0 mM) for 24 h (ambient temperature). After removal from the solution, the functionalized electrodes were washed with DMSO and EtOH, then dried using a heat gun (~80 °C). Then, each electrode was dipped in a solution of [Cu($L_{ancillary}$)$_2$][PF$_6$] where $L_{ancillary}$ = **1**, **2**, **3** or **4** (CH_2Cl_2, 0.1 mM) for 3 days. For co-sensitization, the electrodes functionalized with **5** were immersed in a solution of a 1 : 1 mixture of [Cu(**1**)$_2$][PF$_6$] and [Cu(**3**)$_2$][PF$_6$] (CH_2Cl_2, 0.1 mM for each complex) for 3 days, or were placed sequentially into dye baths containing [Cu(**1**)$_2$][PF$_6$] or [Cu(**3**)$_2$][PF$_6$] (CH_2Cl_2, 0.1 mM) for 3 days. After removal from the dye-bath, the now orange electrodes were washed with CH_2Cl_2 and dried using a heat gun (~80 °C). An N719 reference electrode was made by dipping a Solaronix Test Cell Titania Electrode in a solution (EtOH, 0.3 mM) of N719 (Solaronix) for 3 days. The electrode was removed from the dye-bath, washed with EtOH and dried with a heat gun (~80 °C). Solaronix Test Cell Platinum Electrodes were used for the counter electrodes; volatile organic impurities were removed by placing the electrodes on a heating plate (450 °C, 30 min).

The working and counter electrodes were joined using thermoplast hot-melt sealing foil (Solaronix Test Cell Gaskets) by heating while pressing them together. Electrolyte composition: LiI (0.1 M), I_2 (0.05 M), 1-methylbenzimidazole (0.5 M), 1-butyl-3-methylimidazolinium iodide (0.6 M) in 3-methoxypropionitrile. The electrolyte was introduced into the DSC by vacuum backfilling and then the hole in the counter electrode was sealed (Solaronix Test Cell Sealings) and covered (Solaronix Test Cell Caps).

DSC measurements were made by irradiating from the anode side of the cell using a light source SolarSim 150 (100 mW cm^{-2} = 1 sun). The power of the simulated light was calibrated by using a reference Si cell. All DSCs were completely masked[47,48] before measurements were made.

The external quantum efficiency (EQE) measurements were made using a Spe-Quest quantum efficiency setup (Rera Systems, Netherlands) operating with a 100 W halogen lamp

(QTH) and a lambda 300 grating monochromator (Lot Oriel). The monochromatic light was modulated to 3 Hz using a chopper wheel (ThorLabs), and the cell response was amplified with a large dynamic range IV converter (CVI Melles Griot) and then measured with a SR830 DSP Lock-In amplifier (Stanford Research).

Electrochemical impedance spectroscopy (EIS) measurements were carried out on a ModuLab® XM PhotoEchem photoelectrochemical measurement system from Solartron Analytical. The impedance was measured around the open-circuit potential of the cell at different light intensities (590 nm) in the frequency range 0.05 Hz to 400 kHz using an amplitude of 10 mV. The impedance data were analysed using ZView® software from Scribner Associates Inc.

Results and discussion

Synthesis and characterization of the copper complexes

The hybrid ligands **1**–**4** have been previously been reported.[34,35,36,37,38,39] The homoleptic copper(I) complexes were prepared by reaction of the ligands with $[Cu(MeCN)_4][PF_6]$, and $[Cu(\mathbf{1})_2][PF_6]$, $[Cu(\mathbf{2})_2][PF_6]$, $[Cu(\mathbf{3})_2][PF_6]$ and $[Cu(\mathbf{4})_2][PF_6]$ were isolated as red solids in 94.6 to 100% yield. The positive ion electrospray (ESI) mass spectrum of each compound showed a base peak corresponding to $[M–PF_6]^+$ (see experimental section). These were further confirmed in the high resolution ESI mass spectra.

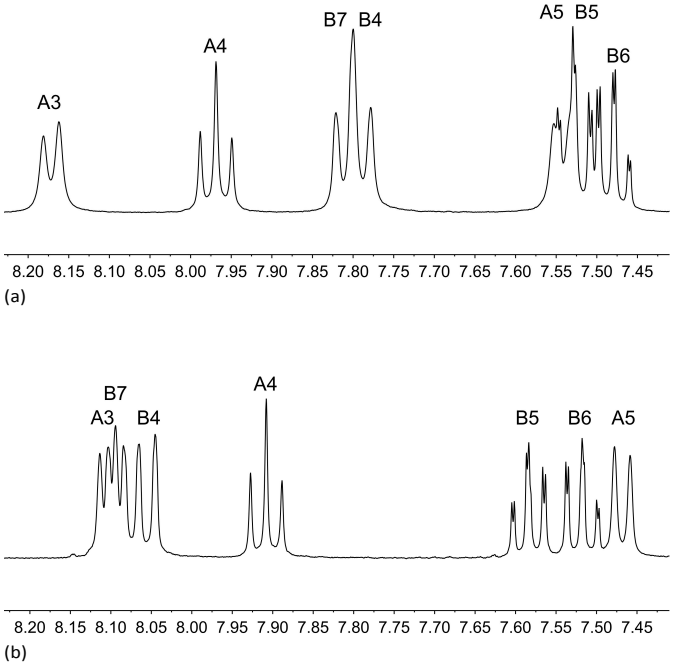

Fig. 1. Aromatic regions of the 500 MHz ^{1}H NMR spectra of (a) $[Cu(\mathbf{2})_2][PF_6]$ and (b) $[Cu(\mathbf{3})_2][PF_6]$ in CD_3CN at 295 K. See Fig. S1 and S2† for the full spectra, and Scheme 1 for proton labels. Chemical shifts in δ / ppm.

^{1}H and ^{13}C NMR spectra of CD_3CN solutions of the complexes were assigned using 2D methods (COSY, NOESY, HMQC and HMBC); for $[Cu(\mathbf{1})_2][PF_6]$, the correlations were made at 220 K. The ^{1}H NMR spectra of $[Cu(\mathbf{2})_2][PF_6]$ and $[Cu(\mathbf{3})_2][PF_6]$ are shown in Fig. 1, S1† and S2† and are well resolved at 295 K. For $[Cu(\mathbf{1})_2][PF_6]$ which contains an imidazolyl NH, all the signals in the room temperature ^{1}H NMR spectrum (in CD_3CN or acetone-d_6) are broad; the NH group gives rise to a broad signal centred at δ 11.7 ppm. The signals sharpen upon cooling to 220 K (Fig. 2), and we propose that the temperature dependence of the spectrum arises from a dynamic process (on–off coordination) involving tautomers of the imidazole unit coupled with rotation about the $C_{pyridine}$–$C_{imidazole}$ bond. The ^{1}H NMR spectra recorded below 245 K show evidence for a minor component (Fig. 2). Fig. 3 shows a comparison of the spectra of acetone-d_6 solution of $[Cu(\mathbf{1})_2][PF_6]$ at 220 K and of ligand **1** at 295 K. The coincidence between the broad signal at δ 8.18 ppm in Fig. 3a with the doublet at δ 8.20 ppm in Fig. 3b suggests that the subspectrum arises from dissociated ligand; the shift in the signal for the NH proton (Fig. 3a *vs* 3b) probably indicating the differing hydrogen bonding environment. Replacing the NH by NMe on going from $[Cu(\mathbf{1})_2][PF_6]$ to $[Cu(\mathbf{4})_2][PF_6]$ leads to a well resolved ^{1}H NMR spectrum at 295 K, and this supports the proposal that the dynamic behaviour in $[Cu(\mathbf{1})_2][PF_6]$ involves the imidazole NH group. $[Cu(\mathbf{1})_2][PF_6]$ must be stored under argon, and solutions of red $[Cu(\mathbf{1})_2][PF_6]$ which are left standing in air slowly oxidize to the corresponding green copper(II) complex. The presence of the $[Cu(\mathbf{1})_2]^{2+}$ cation is supported by a peak envelope in the ESI MS at *m/z* 240.4 showing a characteristic isotope pattern with peaks at half-mass separations.

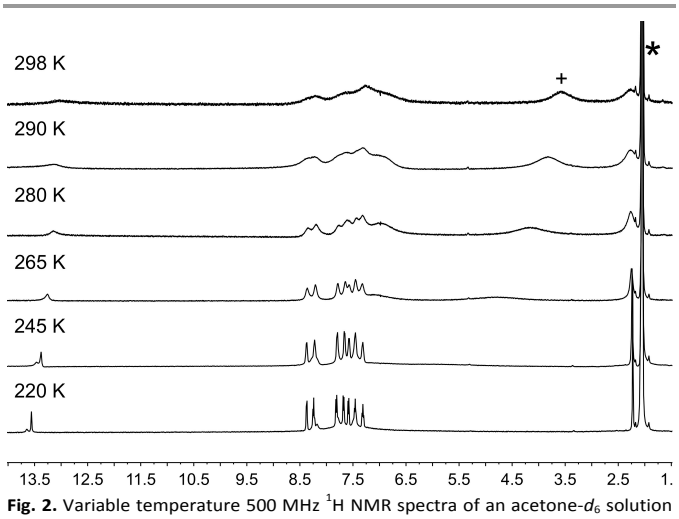

Fig. 2. Variable temperature 500 MHz ^{1}H NMR spectra of an acetone-d_6 solution of $[Cu(\mathbf{1})_2][PF_6]$. * = residual $CD_3(CHD_2)CO$. + = water. Chemical shifts in δ / ppm.

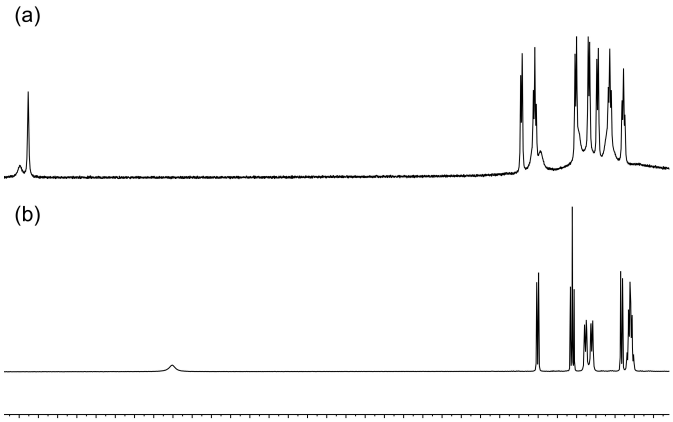

Fig. 3. Comparison of the aromatic regions of the 500 MHz ^{1}H NMR spectra of (a) [Cu(**1**)$_2$][PF$_6$] at 220K and (b) **1** at 295 K, both in acetone-d_6. Chemical shifts in δ / ppm.

Single crystals of [Cu(**2**)$_2$][PF$_6$]·0.5CH$_2$Cl$_2$ and [Cu(**3**)$_2$][PF$_6$] were grown by slow diffusion of Et$_2$O into CH$_2$Cl$_2$ solutions of the compounds. The compounds crystallize in the monoclinic space groups $C2/c$ and $P2_1/c$, respectively, and the structures of the [Cu(**2**)$_2$]$^+$ and [Cu(**3**)$_2$]$^+$ cations are shown in Fig. 4 and 5. The structure determinations confirm that each of **2** and **3** coordinates in an *N,N'*-chelating mode. Atom Cu1 in each cation is tetrahedrally sited and N–Cu–N bond angles are given in the captions to Fig. 4 and 5. The Cu–N bond lengths are typical (range 2.033(4) to 2.074(5) Å) and the angle between the least squares planes through the individual ligands in [Cu(**2**)$_2$]$^+$ is 76.7° and the corresponding angle in [Cu(**3**)$_2$]$^+$ is 86.1°. The [Cu(**2**)$_2$]$^+$ cations form columns along the *c*-axis with face-to-face π-interactions between 1,3-benzoxazole units (Fig. 6). Adjacent pairs of 1,3-benzoxazoles are mutually offset and are related, alternately, by inversion or a 2-fold axis. For the former π-stacking interaction, the distance between the least squares planes through the 1,3-benzoxazoles is 3.23 Å, and the centroid...centroid distance is 3.51 Å. For the latter, the angle between least squares planes is 3.7°, and centroid...plane and centroid...centroid distances are 3.25 and 3.61 Å. The packing of cations in [Cu(**3**)$_2$][PF$_6$] involves centrosymmetric embraces of cations in which the methyl groups point into the thiazole rings (Fig. 6b); the closest CH...thiazole$_{centroid}$ distance is 3.17 Å.[49] In addition, the pyridine ring containing N4 engages in a weak π-stacking contact with the arene ring containing C19^i (symmetry code i = 1–x, –$^1/_2$+y, $^1/_2$–z) in the adjacent molecule; interaction is not optimal, with centroid...centroid and centroid...plane separations of 3.84 and 3.47 Å, respectively, and an angle between the ring planes of 9.9°.

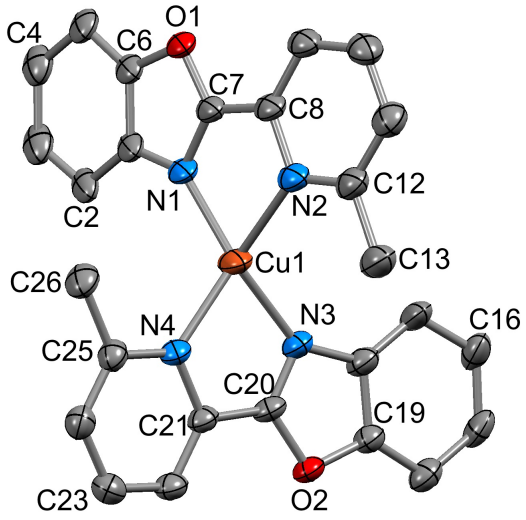

Fig.4. The structure of the [Cu(**2**)$_2$]$^+$ cation in [Cu(**2**)$_2$][PF$_6$]·0.5CH$_2$Cl$_2$. Ellipsoids are plotted at 30% probability level; H atoms and solvent molecules are omitted. Selected bond parameters: Cu1–N1 = 2.060(5), Cu1–N2 = 2.074(5), Cu1–N3 = 2.058(4), Cu1–N4 = 2.047(4), C6–O1 = 1.389(7), C7–O1 = 1.351(6), C19–O2 = 1.389(6), C20–O2 = 1.357(6) Å; N1–Cu1–N2 = 82.12(18), N1–Cu1–N3 = 128.54(19), N2–Cu1–N3 = 117.06(17), N1–Cu1–N4 = 121.62(16), N2–Cu1–N4 = 132.21(18), N3–Cu1–N4 = 81.88(16), C6–O1–C7 = 103.9(4), C19–O2–C20 = 104.5(4)°.

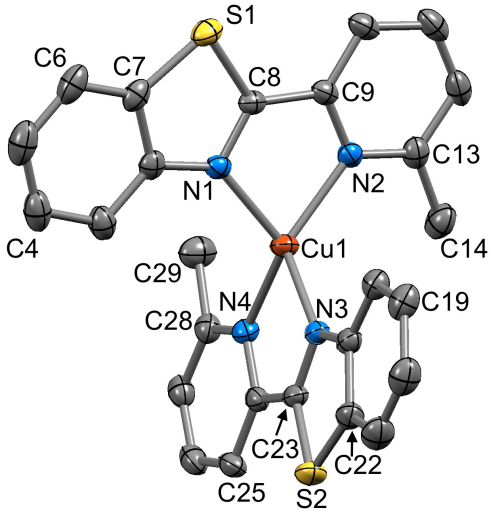

Fig. 5. The structure of the [Cu(**3**)$_2$]$^+$ cation in [Cu(**3**)$_2$][PF$_6$]; ellipsoids are plotted at 30% probability level and H atoms are omitted. Selected bond parameters: Cu1–N1 = 2.043(4), Cu1–N2 = 2.044(4), Cu1–N3 = 2.060(4), Cu1–N4 = 2.033(4), S1–C7 = 1.735(6), S1–C8 = 1.730(4), S2–C22 = 1.736(6), S2–C23 = 1.738(4) Å; N1–Cu1–N2 = 81.54(15), N1–Cu1–N3 = 116.08(15), N2–Cu1–N3 = 122.69(15), N1–Cu1–N4 = 124.03(16), N2–Cu1–N4 = 135.07(16), N3–Cu1–N4 = 81.73(16), C7–S1–C8 = 88.7(2), C22–S2–C23 = 89.1(2)°.

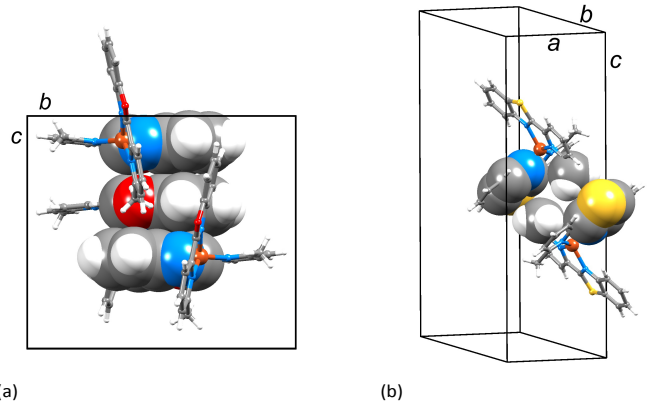

Fig. 6. (a) View down the *a*-axis of the unit cell in $[Cu(\mathbf{2})_2][PF_6]\cdot 0.5CH_2Cl_2$ showing stacked cations. (b) Centrosymmetric embrace of cations in $[Cu(\mathbf{3})_2][PF_6]$.

Solution absorption spectra and electrochemistry

Fig. 7 shows the solution absorption spectra of the four homoleptic copper(I) complexes; absorption maxima are given in the Experimental Section. High-energy bands arise from ligand-based $\pi^*\leftarrow\pi$ and $\pi^*\leftarrow n$ transitions, and the broad absorption between 400 and 520 nm is assigned to a metal-to-ligand charge transfer (MLCT) band. The MLCT absorption maxima, λ_{max}, shift to signficantly to lower energy as the heteroatom in the ligand is changed: O, 424 nm; NH, 435 nm; NMe, 446 nm; S, 465 nm. The intensity of the MLCT band is greatest with the benzothiazole ligand **3** (Fig. 7).

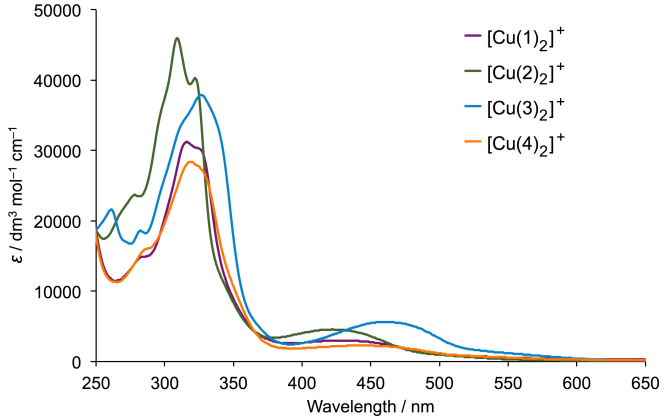

Fig. 7. Solution absorption spectra (in CH_2Cl_2, 1×10^{-5} mol dm^{-3}) of $[Cu(\mathbf{1})_2][PF_6]$, $[Cu(\mathbf{2})_2][PF_6]$, $[Cu(\mathbf{3})_2][PF_6]$ and $[Cu(\mathbf{4})_2][PF_6]$.

The redox activities of $[CuL_2][PF_6]$ (L = **1**, **2**, **3** or **4**) were investigated by cyclic voltammetry of CH_2Cl_2 solutions and a representative cyclic voltammogram (CV) is depicted in Fig. 8. Each complex shows a reversible metal-centred oxidation process (Table 1) assigned to the Cu^+/Cu^{2+} redox couple. The potentials for $[Cu(\mathbf{1})_2][PF_6]$ and $[Cu(\mathbf{4})_2][PF_6]$ (differing only in NH *vs* NMe) are similar, and are also similar to that for $[Cu(dmbpy)_2][PF_6]$ (+0.17 V in CH_3CN).[50] Introduction of O or S heteroatoms on going to $[Cu(\mathbf{2})_2][PF_6]$ or $[Cu(\mathbf{3})_2][PF_6]$, respectively, shifts the copper(I) oxidation to higher potential (Table 1), indicating a better π-acceptor ability, consistent with the red shift in the absorption spectrum of **3.** The four copper(I) complexes show poorly defined reduction processes as presented for $[Cu(\mathbf{4})_2][PF_6]$ in Fig. 8. For $[Cu(\mathbf{1})_2][PF_6]$ and $[Cu(\mathbf{4})_2][PF_6]$, no significant changes in the CV were observed through three successive cycles, whereas both $[Cu(\mathbf{2})_2][PF_6]$ and $[Cu(\mathbf{3})_2][PF_6]$ developed an additional irreversible process at positive potential in subsequent scans. The trend in oxidation potentials is consistent with that observed on going from $[Ru(bpy)_2(L\text{-}NMe)]^{2+}$ to $[Ru(bpy)_2(L\text{-}S)]^{2+}$ (E^{ox} = +1.13 and +1.37 V, respectively, *vs* SCE where L-NMe = 2-(2-pyridyl)-1-methylbenzimidazole and L-S = 2-(2-pyridyl)benzothiazole).[51]

Table 1. Cyclic voltammetric data for copper(I) complexes with respect to Fc/Fc^+; CH_2Cl_2 solutions with $[^nBu_4N][PF_6]$ as the supporting electrolyte and a scan rate of 0.1 V s^{-1}. Processes are near-reversible or reversible.

Complex	$E^{ox}_{1/2}$ / V	$E_{pc} - E_{pa}$ /mV
$[Cu(\mathbf{1})_2][PF_6]$	+0.15	77
$[Cu(\mathbf{2})_2][PF_6]$	+0.41	93
$[Cu(\mathbf{3})_2][PF_6]$	+0.43	82
$[Cu(\mathbf{4})_2][PF_6]$	+0.13	105

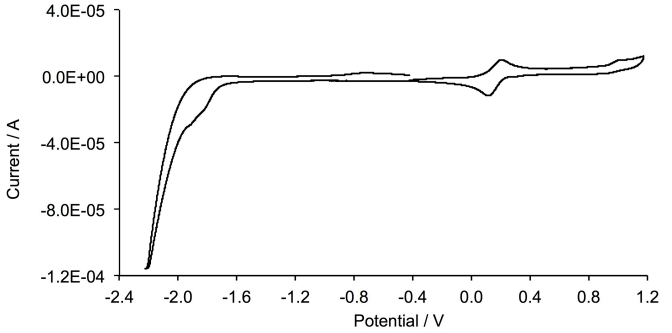

Fig. 8. Cyclic voltammogram for a CH_2Cl_2 solution of $[Cu(\mathbf{4})_2][PF_6]$; scan rate 0.1 V s^{-1} and referenced to Fc/Fc^+.

Solid-state absorption spectra of adsorbed dyes

Transparent FTO/TiO_2 electrodes were functionalized with a heteroleptic copper(I) dye using our established 'surface-as-ligand' strategy.[28] The electrodes were immersed in a DMSO solution of the anchoring ligand **5** (Scheme 1), dried, and then dipped in a CH_2Cl_2 solution of the appropriate homoleptic complex $[Cu(\mathbf{1})_2][PF_6]$, $[Cu(\mathbf{2})_2][PF_6]$, $[Cu(\mathbf{3})_2][PF_6]$ or $[Cu(\mathbf{4})_2][PF_6]$. The solid-state absorption spectra of the surface-assembled dyes $[Cu(\mathbf{5})(\mathbf{1})]^+$ (λ_{max} ~ 443 nm), $[Cu(\mathbf{5})(\mathbf{2})]^+$ (λ_{max} ~ 445 nm), $[Cu(\mathbf{5})(\mathbf{3})]^+$ (λ_{max} ~ 471 nm) and $[Cu(\mathbf{5})(\mathbf{4})]^+$ (λ_{max} ~ 453 nm) are presented in Fig. 9. The absorption maxima for the MLCT bands of the surface-adsorbed heteroleptic dyes are red-shifted with respect to the solution spectra of the homoleptic complexes shown in Fig. 7. The benzothiazole-containing dye exhibits the lowest energy MLCT band, with an absorption tail to ~600 nm (Fig. 9).

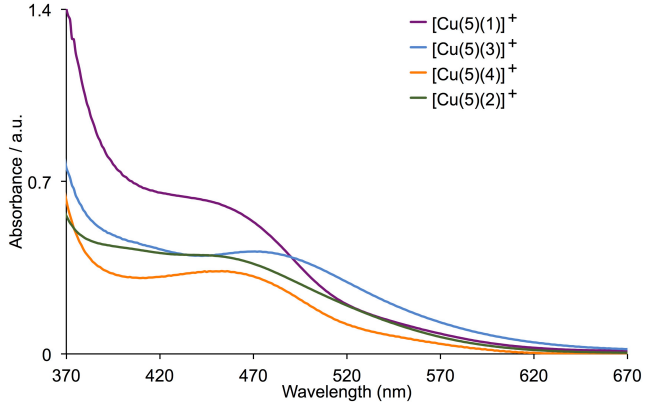

Fig. 9. Solid-state absorption spectra of FTO/TiO_2 electrodes functionalized with $[Cu(\mathbf{5})(\mathbf{1})]^+$, $[Cu(\mathbf{5})(\mathbf{2})]^+$, $[Cu(\mathbf{5})(\mathbf{3})]^+$ or $[Cu(\mathbf{5})(\mathbf{4})]^+$.

Table 2. Performance parameters for DSCs with surface-bound dyes $[Cu(\mathbf{5})(L)]^+$ (L = **1**, **2**, **3** or **4**). See also Table S1†.

Dye	J_{SC} / mA cm^{-2}	V_{OC} / mV	*ff* / %	η / %	Relative η / %
	Day 0 (day of fabricating the DSC)				
$[Cu(\mathbf{5})(\mathbf{1})]^+$	6.93	608	71.9	3.03	40.1
$[Cu(\mathbf{5})(\mathbf{2})]^+$	6.91	531	71.4	2.62	34.7
$[Cu(\mathbf{5})(\mathbf{3})]^+$	7.76	530	69.9	2.88	38.1
$[Cu(\mathbf{5})(\mathbf{4})]^+$	6.99	558	69.5	2.71	35.9
N719	16.57	630	72.4	7.55	100
	Day 7				
$[Cu(\mathbf{5})(\mathbf{1})]^+$	7.16	607	71.9	3.12	45.4
$[Cu(\mathbf{5})(\mathbf{2})]^+$	6.40	579	66.7	2.47	36.0
$[Cu(\mathbf{5})(\mathbf{3})]^+$	7.42	558	62.6	2.59	37.7
$[Cu(\mathbf{5})(\mathbf{4})]^+$	6.74	552	69.8	2.60	37.8
N719	14.47	650	73.0	6.87	100

DSC performances with single dyes

Duplicate DSCs were assembled (see Experimental Section) with surface-bound dyes $[Cu(\mathbf{5})(\mathbf{1})]^+$, $[Cu(\mathbf{5})(\mathbf{2})]^+$, $[Cu(\mathbf{5})(\mathbf{3})]^+$ or $[Cu(\mathbf{5})(\mathbf{4})]^+$. The performances of masked cells are summarized in Table S1†, and Table 2 gives the characteristics of the better performing cell of each duplicate pair. The data confirm that the devices remain stable over a period of a week and values of J_{SC}, V_{OC} and η for duplicate DSCs (Table S1†) confirm the reproducibility of the measurements. The slight improvement in efficency on going from day 0 to 7 (Table 2) follows trends previously observed from other copper(I) sensitizers.[28,31,52] Similar enhancement has been observed for ruthenium(II) dyes and is most likely associated with the initial formation of aggregates of the dye molecules on the surface followed by molecular reorganization over periods of days.[53,54,55] The performance of one DSC containing $[Cu(\mathbf{5})(\mathbf{2})]^+$ was tested after the cell had been stored in the dark for 9 months; values of J_{SC}, V_{OC} and η were 6.40 mA cm^{-2}, 579 mV and 2.47%, emphasizing the long-term stability of the device.

Values of J_{SC}, V_{OC} and η in Table 2 are compared to those for a reference DSC containing the standard ruthenium dye N719, and the final column in Table 2 gives a relative η with respect to 100% for N719. We routinely use this practice to allow valid comparisons between measurements on different sun simulators and with different transparent metal oxide assemblies.[56] Fig. 10 shows *J*–*V* curves for DSCs containing dyes $[Cu(\mathbf{5})(L)]^+$ with L = **1**, **2**, **3** or **4**. All DSCs exhibit good fill-factors (*ff*) which contributes to overall photoconversion efficiencies of between 2.62% for $[Cu(\mathbf{5})(\mathbf{2})]^+$ to 3.03% for $[Cu(\mathbf{5})(\mathbf{1})]^+$ on the initial day (Table 2). External quantum efficiency (EQE) data are presented in Table 3 and Fig. 11, and reveal that all dyes give EQE_{max} of 53–55%. The EQE spectra all exhibit λ_{max} = 480 nm, despite the variation (443–471 nm) observed in the broad MLCT solid-state absorption spectra of the dyes. Since the presence of protons at the TiO_2 surface is known to influence dye performance,[57,58] we were interested to compare the performances of DSCs sensitized by $[Cu(\mathbf{5})(\mathbf{1})]^+$ and $[Cu(\mathbf{5})(\mathbf{4})]^+$. Data in Tables 2 and S1† reveal little change in the values of J_{SC} on replacing the imidazolyl NH by NMe, but rather a drop in V_{OC} of ~50 mV; the near overlap of the EQE spectra (Fig. 11) is consistent with the small differences observed in the values of J_{SC}. We note in passing that the protonation microstate of anchoring ligand **5** on the semiconductor surface is not known.

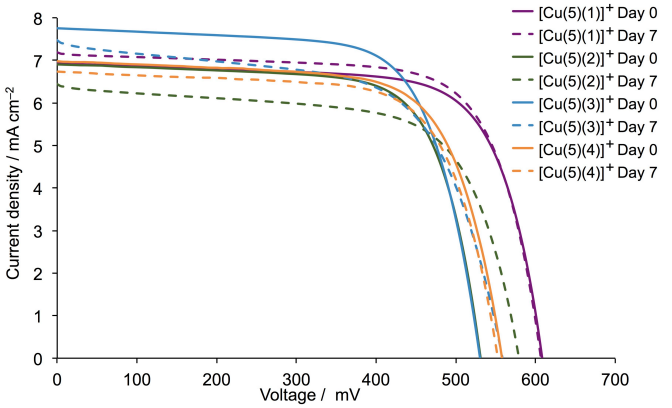

Fig. 10. *J*–*V* curves for the DSCs given in Table 1 with dyes $[Cu(\mathbf{5})(L)]^+$ (L = **1**, **2**, **3** or **4**). Curves were recorded on the day of cell assembly (day 0) and 7 days later.

Table 3. EQE maxima for DSCs with dyes $[Cu(\mathbf{5})(L)]^+$ (L = **1**, **2**, **3** or **4**) and with co-sensitization using $[Cu(\mathbf{5})(\mathbf{1})]^+$ and $[Cu(\mathbf{5})(\mathbf{3})]^+$. Data are for the better of two duplicate cells; see Table S1† for complete data.

	Day 0		Day 7	
	EQE_{max} / %	λ_{max} / nm	EQE_{max} / %	λ_{max} / nm
$[Cu(\mathbf{5})(\mathbf{1})]^+$	53.0	480	54.7	480
$[Cu(\mathbf{5})(\mathbf{2})]^+$	54.1	480	50.5	470
$[Cu(\mathbf{5})(\mathbf{3})]^+$	53.8	480	46.2	470
$[Cu(\mathbf{5})(\mathbf{4})]^+$	55.3	480	54.0	480
N719	71.8	540	71.1	540

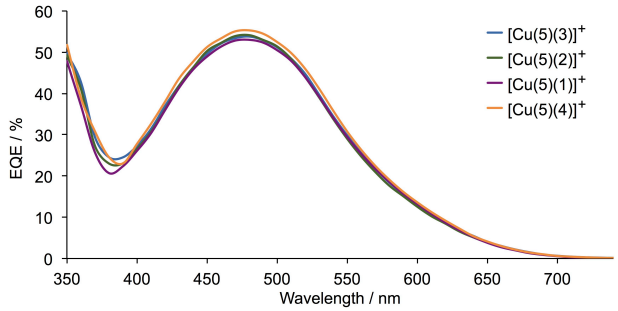

Fig. 11. EQE spectra recorded on the day of cell assembly (day 0) for the DSCs given in Table 3 with dyes $[Cu(\mathbf{5})(L)]^+$ (L = **1**, **2**, **3** or **4**).

Of particular note in Fig. 10 is that ancillary ligand **3** (S-containing) leads to the highest short-circuit current density (7.76 mA cm^{-2}), while the open-circuit voltage is optimized when the ancillary ligand is **1** (NH-containing). This suggested to us that there could be benefits in using a mixed dye co-sensitized approach.

Co-sensitization: solid-state absorption spectra of dye-functionalized electrodes

Transparent FTO/TiO_2 electrodes were functionalized with anchor **5** and then immersed in a CH_2Cl_2 solution containing a 1:1 mixture of $[Cu(\mathbf{1})_2][PF_6]$ and $[Cu(\mathbf{3})_2][PF_6]$. Fig. 12a compares the solid-state absorption spectra of these electrodes with those functionalized with the complexes $[Cu(\mathbf{5})(\mathbf{1})]^+$ or $[Cu(\mathbf{5})(\mathbf{3})]^+$. Compared to values of λ_{max} of 443 and 471 nm, respectively, for the single dyes, the co-sensitized surface has an absorption maximum at ~440 nm, most reminiscent of $[Cu(\mathbf{5})(\mathbf{1})]^+$. This suggested that competition between the dyes in the 1:1 mixture leads to preferential coverage with $[Cu(\mathbf{5})(\mathbf{1})]^+$ rather than a mixture of $[Cu(\mathbf{5})(\mathbf{1})]^+$ and $[Cu(\mathbf{5})(\mathbf{3})]^+$ and that dye-bath solution composition is not reflected in the composition of dyes on the surface. This is supported by the DSC measurements (see later). We then investigated the solid-state absorption spectra of FTO/TiO_2 electrodes functionalized with **5** which were then sequentially dipped in dye baths containing $[Cu(\mathbf{1})_2][PF_6]$ and then $[Cu(\mathbf{3})_2][PF_6]$ (Fig. 12b, co-sensitized '**1** then **3**') or $[Cu(\mathbf{3})_2][PF_6]$ and then $[Cu(\mathbf{1})_2][PF_6]$ (Fig. 12b, co-sensitized '**3** then **1**'). For the latter, the solid-state absorption spectrum maximum at λ_{max} = 442 nm replicates that of the single dye $[Cu(\mathbf{5})(\mathbf{1})]^+$ (443 nm), again consistent with replacement of surface-coordinated **3** by **1** in the second dye-bath. In contrast, the broad MLCT absorption for co-sensitized surface '**1** then **3**' (Fig. 12b, green curve) with λ_{max} ~460 nm suggests that both dyes $[Cu(\mathbf{5})(\mathbf{1})]^+$ and $[Cu(\mathbf{5})(\mathbf{3})]^+$ are bound to the TiO_2. Taken in conjunction with the solution UV-VIS spectroscopic data and solution electrochemical data reported earlier, this suggests that **1** is a significantly stronger σ-donor than **3**.

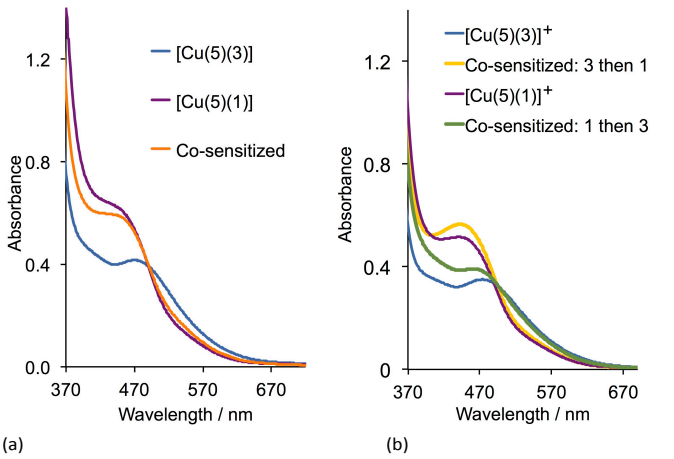

Fig. 12. Solid-state absorption spectra of FTO/TiO_2 electrodes functionalized with single dyes $[Cu(\mathbf{5})(\mathbf{1})]^+$ (purple line) or $[Cu(\mathbf{5})(\mathbf{3})]^+$ (blue line) compared with (a) electrodes functionalized with **5** and then treated with a 1:1 mixture of $[Cu(\mathbf{1})_2][PF_6]$ and $[Cu(\mathbf{3})_2][PF_6]$ (co-sensitized, orange line); (b) **5** and then treated sequentially with $[Cu(\mathbf{1})_2][PF_6]$ then $[Cu(\mathbf{3})_2][PF_6]$ (green line) or $[Cu(\mathbf{3})_2][PF_6]$ then $[Cu(\mathbf{1})_2][PF_6]$ (yellow line).

Co-sensitization: DSC performances

FTO/TiO_2 electrodes with a scattering layer (Solaronix Test Cell Titania) were functionalized with anchor **5** and then immersed in a dye bath containing a 1:1 mixture of $[Cu(\mathbf{1})_2][PF_6]$ and $[Cu(\mathbf{3})_2][PF_6]$, or sequentially in dye baths containing $[Cu(\mathbf{1})_2][PF_6]$ followed by $[Cu(\mathbf{3})_2][PF_6]$, or $[Cu(\mathbf{3})_2][PF_6]$ followed by $[Cu(\mathbf{1})_2][PF_6]$ (Fig. 12b, co-sensitized '**3** then **1**'). The active dyes in every case were $[Cu(\mathbf{5})(\mathbf{1})]^+$ or $[Cu(\mathbf{5})(\mathbf{3})]^+$, arising from the exchange reactions:

FTO/TiO_2/(**5**) + $[Cu(\mathbf{1})_2]^+$ ➔ FTO/TiO_2/$[(\mathbf{5})Cu(\mathbf{1})]^+$ + **1**

FTO/TiO_2/(**5**) + $[Cu(\mathbf{3})_2]^+$ ➔ FTO/TiO_2/$[(\mathbf{5})Cu(\mathbf{3})]^+$ + **3**

All measurements were carried out in duplicate and the performance data for the better performing of each pair of co-sensitized DSCs are given in Table 4. The complete data set is presented in Table S2†, and *J-V* curves are shown in Fig. 13.

We first consider the use of the 1:1 dye-bath. A comparison of the performances of the single-dye-containing DSCs (Table 2) with those of the co-sensitized cells shows that the high V_{OC} values of DSCs sensitized with only $[Cu(\mathbf{5})(\mathbf{1})]^+$ are also observed for the co-sensitized cells. The small gain in J_{SC} (6.93 to 7.20 mA cm^{-2}) is consistent with a small increase in EQE_{max} (53.0%, Table 3 to 56.8%, Table 4). The latter is maintained over a period of a week after fabricating the cells. While the overall efficiencies of ~3% (Tables 4 and S2†) are satisfyingly 40% that of the N719 reference DSC and the cells are stable over a period of a week (Fig. 13, orange curves), there is no noticeable enhancement with respect to the DSCs sensitized with $[Cu(\mathbf{5})(\mathbf{1})]^+$ alone and, taken with the solid-state absorption data, suggest that surface-coverage by $[Cu(\mathbf{5})(\mathbf{1})]^+$ is dominant when the electrode functionalized with anchor **5** is exposed to both $[Cu(\mathbf{1})_2]^+$ and $[Cu(\mathbf{3})_2]^+$.

Next, we consider electrodes functionalized with **5** that are treated sequentially with $[Cu(\mathbf{3})_2]^+$ and then $[Cu(\mathbf{1})_2]^+$. The performances of these DSCs are rather similar to those

Table 4. Performance parameters and EQE maxima for DSCs with co-sensitization. See Table S2† for data for duplicate DSCs in days 0, 3 and 7.

Dye-bath or baths[a]	J_{SC} / mA cm^{-2}	V_{OC} / mV	*ff* / %	η / %	Relative η / %	EQE max / nm, %
Day 0 (day of fabricating the DSC)						
1:1 mixture of $[Cu(\mathbf{1})_2]^+$ and $[Cu(\mathbf{3})_2]^+$	7.20	592	70.9	3.02	40.0	480, 56.8
$[Cu(\mathbf{3})_2]^+$ followed by $[Cu(\mathbf{1})_2]^+$	6.91	588	72.8	2.96	39.2	480, 51.3
$[Cu(\mathbf{1})_2]^+$ followed by $[Cu(\mathbf{3})_2]^+$	6.35	528	72.8	2.44	32.3	460, 40.6
N719	16.57	630	72.4	7.55	100	540, 71.8
Day 7						
1:1 mixture of $[Cu(\mathbf{1})_2]^+$ and $[Cu(\mathbf{3})_2]^+$	7.30	600	70.7	3.10	45.1	470, 56.8
$[Cu(\mathbf{3})_2]^+$ followed by $[Cu(\mathbf{1})_2]^+$	6.24	586	71.9	2.63	38.3	480, 48.5
$[Cu(\mathbf{1})_2]^+$ followed by $[Cu(\mathbf{3})_2]^+$	5.95	521	71.7	2.22	32.3	480, 46.4
N719	14.47	650	73.0	6.87	100	540, 71.1

[a]See text for description of dye assembly.

fabricated using the mixed dye-bath (Tables 4 and S2†). Again, values of J_{SC} and V_{OC}, the EQE_{max} and solid-state absorption spectra are all consistent with the dominant dye being $[Cu(\mathbf{5})(\mathbf{1})]^+$. Exposing the anchor-functionalized electrodes to the homoleptic copper(I) complexes in the reverse order, (i.e. $[Cu(\mathbf{1})_2]^+$ then $[Cu(\mathbf{3})_2]^+$) results in poorer performing DSCs. The high values of J_{SC} that were characteristic of the single S-containing dye $[Cu(\mathbf{5})(\mathbf{3})]^+$ are not observed for the mixed dye system. The values of V_{OC} for DSCs with dyes assemblied by the '**3** then **1**' procedure are close to those obtained when the dyes are assembled using the 1 : 1 mixture of $[Cu(\mathbf{1})_2][PF_6]$ and $[Cu(\mathbf{3})_2][PF_6]$ in the dye-bath (Fig. 13). Moreover, the V_{OC} values replicate those observed for the DSCs with the single dye $[Cu(\mathbf{5})(\mathbf{1})]^+$. In contrast, V_{OC} values for DSCs with dyes assemblied by the '**1** then **3**' method are similar to those of DSCs with single dye $[Cu(\mathbf{5})(\mathbf{3})]^+$. The results from this part of the investigation are consistent with competition for surface binding-sites with ligand **1** dominating over **3**, both in binding and in contribution to the overall photoresponse.

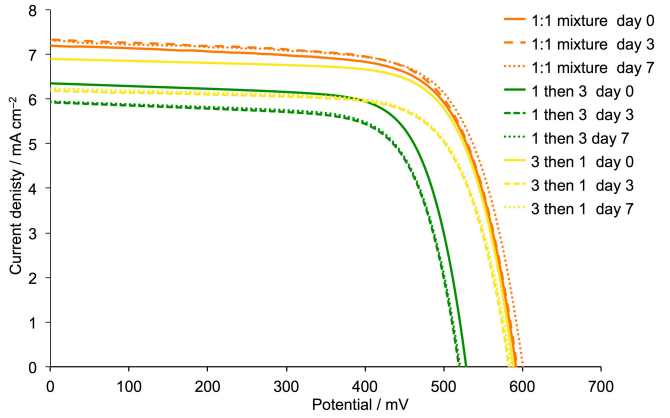

Fig. 13. *J–V* curves for the DSCs given in Table 4. Curves were recorded on the day of cell assembly (day 0), then 3 and 7 days later. The legend abbreviations correspond to the explanation given in the left-hand column of Table 4.

Electrochemical impedance spectroscopy (EIS): introduction

From the underlying principles set out by Heaviside at the end of the 19th century, electrochemical impedance spectroscopy (EIS) has developed into a valuable tool for investigating the mechanisms of electrochemical reactions and determining dielectric and transport properties of materials.[59] In addition to applications in the study of reaction mechanisms, corrosion and surface processes, semiconductors and batteries,[60] EIS plays an important role in investigating physical processes within DSCs.[61,62,63] For example, key parameters including recombination resistance (R_{rec}), transport resistance (R_{tr}) and chemical capacitance (C_{μ}) can be extracted from EIS data.

EIS measurements may be made with an adjustable light source in order to investigate the effect of illumination intensity, using a potentiostat to apply a small AC current of varied frequency. While measuring near V_{OC} conditions, the resulting impedance response is recorded as a function of light intensity and applied frequency. The data are usually represented in a Nyquist plot (Fig. 14) in which, ideally, three separate semi-circles are observed. Each semi-circle corresponds to the impedance of a specific interfacial charge transfer process occurring at a given frequency. Starting at the origin of the Nyquist plot, the distance from zero to the start of the first semi-circle describes the series resistance (R_s) within the whole measurement. This arises predominantly from the charge resistance of the TiO_2/FTO interface.[64] The first semi-circle displays the cathode/electrolyte charge transfer resistance (R_{Pt}), the second the recombination resistance of the active layer/electrolyte interface (R_{rec}) and the third corresponds to the diffusion resistance of the charge carriers within the electrolyte (R_d). The semi-circle corresponding to R_d may be hidden due to overlapping with the R_{rec} semi-circle.[65]

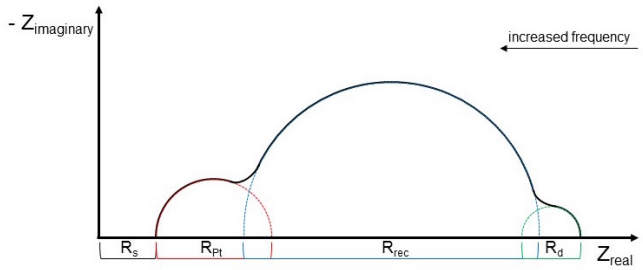

Fig. 14. A schematic diagram of a Nyquist plot of a well functioning DSC at high light intensity showing overlapping semi-circles which have been extrapolated for clarity.

Fig. 15 displays the equivalent circuit model that we have adopted for the fitting of DSC data. The model consists of five elements. First, an extended distributed element (DX1) was used for fitting of the active layer/electrolyte interface according to the transition line model.[66] A Warburg diffusion element (Ws1) was introduced to model the diffusion impedance of the charge carrier through the electrolyte close to the dye-functionalized semiconductor surface. The sub-circuit containing a series resistance (R1) and a constant phase element (CPE1) models the Pt counter electrode. The constant phase element was used instead of a capacitor circuit element to obtain a better fit taking surface roughness into account which is not the case of an ideal capacitor.[67] A further series resistance (R2) was introduced to model the series resistance of the device throughout the entire measurement.

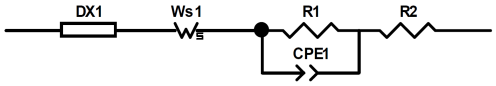

Fig. 15. Equivalent electric circuit used to model EIS data.

In the following discussion, we first consider DSCs containing the single surface-bound dyes $[Cu(\mathbf{5})(\mathbf{1})]^+$, $[Cu(\mathbf{5})(\mathbf{2})]^+$, $[Cu(\mathbf{5})(\mathbf{3})]^+$ or $[Cu(\mathbf{5})(\mathbf{4})]^+$. The influence of the heteroatom is initially investigated, and then the impact of replacing a proton by a methyl group on going from ligand **1** to **4**. Finally, we consider the different co-sensitized DSCs. All EIS measurements were conducted 3 days after sealing the cell. All DSCs utilize the same anchoring ligand **5**, and have identical electrolyte composition as well as TiO_2 semiconductor and counter electrodes.

EIS for DSCs containing $[Cu(5)(1)]^+$, $[Cu(5)(2)]^+$, $[Cu(5)(3)]^+$ or $[Cu(5)(4)]^+$

The key parameters of the EIS measurement at a light intensity of 22 mW cm^{-2} are given in Table 5, and those for a light intensity of 2.2 mW cm^{-2} in Table 6. The data in Table 5 demonstrate that DSCs with $[Cu(\mathbf{5})(\mathbf{1})]^+$, $[Cu(\mathbf{5})(\mathbf{2})]^+$ and $[Cu(\mathbf{5})(\mathbf{3})]^+$ have a higher chemical capacitance (C_μ) and lower recombination resistance (R_{rec}). The higher the capacitance, the higher the total charge density in the TiO_2 semiconductor, and the more electrons reside in the conduction band prior to collection. When the transport resistance (R_{tr}) is also low, a higher J_{SC} is observed because of the higher mobility of electrons and shorter transit times in the semiconductor. The fact that R_{tr} is rather low relative to R_{rec} (see later discussion) in all of the DSCs (Table 6) is shown by the good separation of the first and second semi-circles in the Nyquist plot shown in Fig. 16 and S3†.

Table 5. EIS data obtained from measurements at a light intensity of 22 mW cm^{-2} of DSCs containing the dyes $[Cu(\mathbf{5})(L)]^+$ (L = **1**, **2**, **3** or **4**).

Dye	V_{OC}[a] / mV	R_{rec} / Ω	C_μ / μF	R_{Pt} / Ω	$C_{Pt\mu}$ / μF	τ / ms
$[Cu(\mathbf{5})(\mathbf{1})]^+$	621	159	337	9	6	54
$[Cu(\mathbf{5})(\mathbf{2})]^+$	587	210	298	15	6	62
$[Cu(\mathbf{5})(\mathbf{3})]^+$	554	178	322	20	6	57
$[Cu(\mathbf{5})(\mathbf{4})]^+$	590	189	244	16	5	46

[a] V_{OC} values obtained from the EIS measurements at a given light intensity.

Table 6. EIS data obtained from measurements at a light intensity of 2.2 mW cm^{-2} of DSCs containing the dyes $[Cu(\mathbf{5})(L)]^+$ (L = **1**, **2**, **3** or **4**).

Dye	V_{OC}[a] / mV	R_{rec} / Ω	$C\mu$ / μF	R_{Pt} / Ω	$C_{Pt}\mu$ / μF	R_{tr} / Ω	τ / ms	L_d/ μm
$[Cu(\mathbf{5})(\mathbf{1})]^+$	552	974	170	6	12	124	166	34
$[Cu(\mathbf{5})(\mathbf{2})]^+$	538	1076	168	13	9	129	180	35
$[Cu(\mathbf{5})(\mathbf{3})]^+$	510	893	187	19	7	106	167	35
$[Cu(\mathbf{5})(\mathbf{4})]^+$	504	1014	131	21	6	160	133	30

[a] V_{OC} values obtained from the EIS measurements at a given light intensity.

A comparison of the DSCs containing dyes $[Cu(\mathbf{5})(\mathbf{1})]^+$ and $[Cu(\mathbf{5})(\mathbf{2})]^+$ is instructive. At high light intensities, $[Cu(\mathbf{5})(\mathbf{1})]^+$ leads to a higher C_μ and a lower R_{rec}. However, in this case the negative influence on the performance of the DSC of a low R_{rec} is partly offset by a low R_{tr} (Table 6) with the result that the electrons are easily transported through the semiconductor. This results in the high J_{SC} (6.88 mA cm^{-2} on day 3, see Table S1†) of the DSCs containing the dye $[Cu(\mathbf{5})(\mathbf{1})]^+$. The R_{tr} values are extracted from the EIS measurements at low light intensities (Table 6), because R_{tr} is more dominant at moderate voltages, as is seen in Fig. 17 and S4†. On the other hand, DSCs with ancillary ligand **2** have a low C_μ and a high R_{rec} in conjunction with a comparable R_{tr}. Here, the lowest J_{SC} value (6.19 mA cm^{-2} on day 3, see Table S1†) is observed because fewer electrons are injected to the semiconductor, whilst the electron transport remains comparable to DSCs with ligand **1**. DSCs with **3** have the lowest R_{tr} of all single dye DSCs (see Table 6) but the C_μ and R_{rec} lie in between those of **1** and **2** at high light intensities (see Table 5). This trend is observed in the rather high J_{SC} (6.77 mA cm^{-2} on day 3, see Table S1†) of the DSCs containing the dye $[Cu(\mathbf{5})(\mathbf{3})]^+$ found in the *J–V* measurements (Table 2).

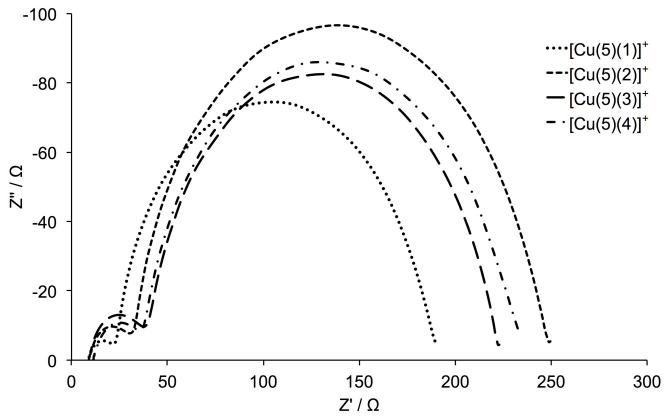

Fig. 16. Nyquist plots of DSCs containing the dyes [Cu(**5**)(L)]$^+$ (L = **1**, **2**, **3** or **4**) at a light intensity of 22 mW cm^{-2}.

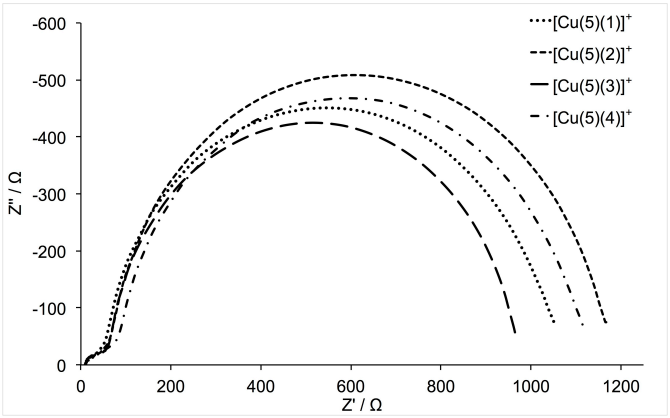

Fig. 17. Nyquist plots of DSCs containing the dyes [Cu(**5**)(L)]$^+$ (L = **1**, **2**, **3** or **4**) at a light intensity of 2.2 mW cm^{-2}.

In a DSC, the theoretical V_{OC} is the difference between the energy level of the redox couple in the electrolyte and the Fermi level (E_F) of the semiconductor. The latter may be altered by increasing or decreasing the conduction band (CB) level; a more negative CB leads to an increase in V_{OC} and *vice versa*. In this study, the I^-/I_3^- electrolyte is constant and observed changes in V_{OC} arise from changes to the CB level of the semiconductor brought about by the variation in dye. As seen in Table 2, the highest V_{OC} is observed with a DSC containing [Cu(**5**)(**1**)]$^+$ and the lowest with [Cu(**5**)(**3**)]$^+$. The trends in the *J–V* curves are also observed in the EIS measurements at a light intensity of 22 mW cm^{-2} under open-circuit voltage conditions. As stated above, more efficient electron injection may result in a higher C_μ. However, a better charge injection is favoured by a more extensive charge compensation which, in turn, results in a lower CB level and, consequently, a lower V_{OC}.[68] In addition to the influence of the charge compensation on the CB level, the electron recombination with the I_3^- in the electrolyte also has an impact. A relatively high C_μ and a high R_{rec} yield a good value for the electron lifetime (τ), calculated as the product of C_μ and R_{rec}. All DSCs show values of τ between 54 and 62 ms. A higher τ implies a lower charge loss in the semiconductor which keeps V_{OC} at a high value. The length of the diffusion path (L_d) for electrons in the semiconductor is also a good parameter to understand the functioning of the device. For a well-functioning cell, L_d should be greater than the thickness of the semiconductor layer. This is the case for all the DSCs studied, even at low light intensities. Table 6 shows that the DSCs have L_d values of 30–35 μm, about three times the thickness of the semiconductor (≈12 μm). In conclusion, the more electrons are accumulated in the semiconductor, the more likely it is that the CB level is shifted to more negative potential and the higher the resulting V_{OC}. The interplay of all of these parameters influence the V_{OC}, although the direct impact of individual parameters cannot be extracted.

We now consider the effect of replacing the imidazolyl NH by NMe in comparing ancillary ligands **1** and **4**. When comparing the *J–V* curves of DSCs containing surface-bound dyes [Cu(**5**)(**1**)]$^+$ or [Cu(**5**)(**4**)]$^+$ (purple and orange curves in Fig. 10), the only significant differences are in V_{OC} (608 mV for [Cu(**5**)(**1**)]$^+$ and 558 mV for [Cu(**5**)(**4**)]$^+$ on the day of sealing the DSCs, and 604 and 555 mV, respectively, on day 3, Table S1†). The EIS measurements (Tables 5 and 6) demonstrate that the DSC with [Cu(**5**)(**1**)]$^+$ has a higher C_μ but a lower R_{rec} and lower R_{tr} than with [Cu(**5**)(**4**)]$^+$. The higher C_μ and the lower R_{tr} of DSCs containing [Cu(**5**)(**1**)]$^+$ *versus* [Cu(**5**)(**4**)]$^+$ should result in a higher J_{SC}. On the other hand, the higher R_{rec} of [Cu(**5**)(**4**)]$^+$ might lead to comparable J_{SC} values (Tables 2 and S1†). The only molecular difference between these dyes is the imidazolyl NH (in **1**) *versus* NMe (in **4**). The higher R_{rec} of the DSC with [Cu(**5**)(**4**)]$^+$ may be an effect of the methyl group shielding the semiconductor surface through increased steric hindrance compared to [Cu(**5**)(**1**)]$^+$. Consequently, less electrolyte can reach the surface to promote recombination reactions between the injected electrons and the electrolyte. The fact that neither a higher C_μ nor higher V_{OC} is associated with ancillary ligand **4** suggests that the presence of the electron-donating Me group does not lead to better charge injection. As stated earlier, the only notable difference between the DSCs containing [Cu(**5**)(**1**)]$^+$ and [Cu(**5**)(**4**)]$^+$ is the V_{OC}. From an EIS point of view, the origin of this difference can be seen in the values of τ and L_d. Both parameters are higher for the DSC containing [Cu(**5**)(**1**)]$^+$. As already discussed, compared to the DSC with [Cu(**5**)(**4**)]$^+$, that with [Cu(**5**)(**1**)]$^+$ benefits from a higher C_μ and lower R_{tr}. Consequently, less electron loss in the semiconductor results in a higher population of electrons in the CB, and as a consequence, a higher E_F and a higher V_{OC}. In conclusion, the high C_μ, low R_{tr}, and good L_d and τ values contribute to the high values of V_{OC} and J_{SC} observed for DSCs with the dye [Cu(**5**)(**1**)]$^+$ (Tables 2 and S1†).

EIS for DSCs co-sensitized with [Cu(5)(1)]$^+$ and [Cu(5)(3)]$^+$

The *J–V* measurements of the DSCs containing [Cu(**5**)(**1**)]$^+$ and [Cu(**5**)(**3**)]$^+$ showed that use of ancillary ligand **1** or **3** leads to

the highest V_{OC} or J_{SC}, respectively. The results of co-sensitization experiments were significantly affected by the different dipping conditions used in the dye-baths, and the latter are expected to have an impact on the EIS parameters. EIS data for co-sensitized DSCs are presented in Tables 7 and 8, and the nomenclature in the left-hand column is the same as in Table 4.

Table 7. EIS data obtained from measurements at a light intensity of 22 mW cm^{-2} of DSCs containing a mixture of dyes with the anchoring ligand **5** and ancillary ligand **1** or **3.**

	V_{OC}[a] / mV	R_{rec} / Ω	C_{μ} / μF	R_{Pt} / Ω	$C_{Pt\mu}$ / μF	τ / ms
1:1 mixture of $[Cu(\mathbf{1})_2]^+$ and $[Cu(\mathbf{3})_2]^+$	634	114	432	20	6	49
$[Cu(\mathbf{3})_2]^+$ followed by $[Cu(\mathbf{1})_2]^+$	623	171	319	14	5	55
$[Cu(\mathbf{1})_2]^+$ followed by $[Cu(\mathbf{3})_2]^+$	556	133	174	21	7	23

[a] V_{OC} values obtained from the EIS measurements at a given light intensity.

Table 8. EIS data obtained from measurements at a light intensity of 2.2 mW cm^{-2} of DSCs containing a mixture of dyes with the anchoring ligand **5** and ancillary ligand **1** or **3.**

Dye	V_{OC}[a] / mV	R_{rec} / Ω	$C\mu$ / μF	R_{Pt} / Ω	$C_{Pt}\mu$ / μF	R_{tr} / Ω	τ / ms	L_d / μm
1:1 mixture of $[Cu(\mathbf{1})_2]^+$ and $[Cu(\mathbf{3})_2]^+$	552	635	238	20	7	71	152	36
$[Cu(\mathbf{3})_2]^+$ followed by $[Cu(\mathbf{1})_2]^+$	562	893	180	15	7	65	161	45
$[Cu(\mathbf{1})_2]^+$ followed by $[Cu(\mathbf{3})_2]^+$	487	-	-	-	-	-	-	-[b]

[a] V_{OC} are values obtained from the EIS measurements at a given light intensity. [b]EIS measurement was not fitted due to high R_{tr} (see text).

DSCs with electrodes functionalized with **5** and then soaked in a dye-bath containing a 1:1 mixture of $[Cu(\mathbf{3})_2]^+$ and $[Cu(\mathbf{1})_2]^+$ gave the highest C_{μ} (Table 7) of all measured DSCs. The high C_{μ} is consistent with the observed high J_{SC} (Table 4). The moderate value of R_{tr} facilitates improved electron transport in the semiconductor which, in turn, enhances J_{SC}. However, the relatively low R_{rec} militates against further enhancement of the value of J_{SC}. The EIS parameters for DSCs with electrodes functionalized with **5** and then soaked sequentially in dye-baths containing $[Cu(\mathbf{3})_2]^+$ then $[Cu(\mathbf{1})_2]^+$ are comparable with those using the 1:1 mixture of $[Cu(\mathbf{3})_2]^+$ and $[Cu(\mathbf{1})_2]^+$ (Tables 7 and 8). Of particular note is the increase in R_{rec} on going from the mixed to sequential dye-baths. Exposing the electrodes with adsorbed anchor **5** to the homoleptic copper(I) complexes in the reverse order, (i.e. $[Cu(\mathbf{1})_2]^+$ then $[Cu(\mathbf{3})_2]^+$) results in the lowest C_{μ} value in this study. In addition, R_{tr} is very high and R_{rec} is rather low. The very large R_{tr} meant that the data could not be fitted with the model in Fig. 15 at a low light intensity (Table 8); a Gerischer circuit element would have been needed in order to produce a good fit. However, this was not carried out since it was sufficient to establish that the R_{tr} of this cell is significantly larger than for the others in the series (Fig. 18 and S5†). The high R_{tr} is reflected in the EIS measurements at high light intensities (Fig. 19 and S6†) where the first and second semi-circle overlap (see earlier discussion). Because of the high R_{tr} and low R_{rec}, the tendency for electron injection into the CB as well as the charge density in the semiconductor are reduced. Additionally, the recombination reaction with the electrolyte is dominant, and electrons in the semiconductor are lost by recombination. It follows that V_{OC} is low for DSCs assembled using the dye-baths in the sequence $[Cu(\mathbf{1})_2]^+$ then $[Cu(\mathbf{3})_2]^+$ (Table 7). Once again, the impact of all EIS parameters on V_{OC} is apparent. The electron lifetime τ for '**1** then **3**' co-sensitized DSCs at high light intensity is 23 ms which is much shorter (Table 7) than those of DSCs made using '**3** then **1**' co-sensitization (τ = 55 ms) or a 1:1 mixture of $[Cu(\mathbf{3})_2]^+$ and $[Cu(\mathbf{1})_2]^+$ (τ = 49 ms). The latter are in the same range as for the DSCs containing the single dyes **1** or **3** (Table 5). Similar trends are observed at lower light intensities (Tables 6 and 8). We note that L_d is, in the case of the DSCs made with a combination of dyes, higher than in the single dye DSCs. The cell with the '**3** then **1**' dipping procedure has a value of L_d = 45 μm which is the highest L_d in this study.

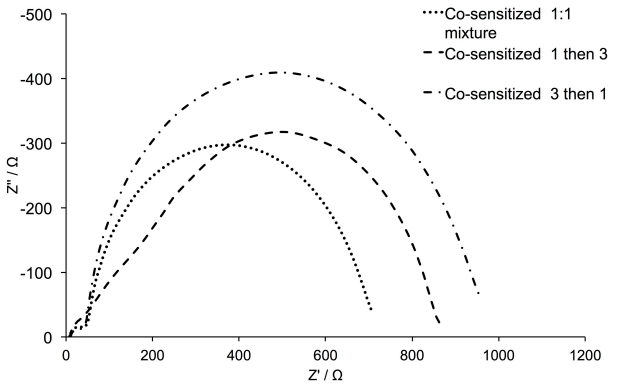

Fig 18. Nyquist plots of DSCs containing mixtures of the dyes $[Cu(\mathbf{5})(\mathbf{1})]^+$ and $[Cu(\mathbf{5})(\mathbf{3})]^+$ at a light intensity of 2.2 mW cm^{-2}. Three different dye-bath procedures were used (see text).

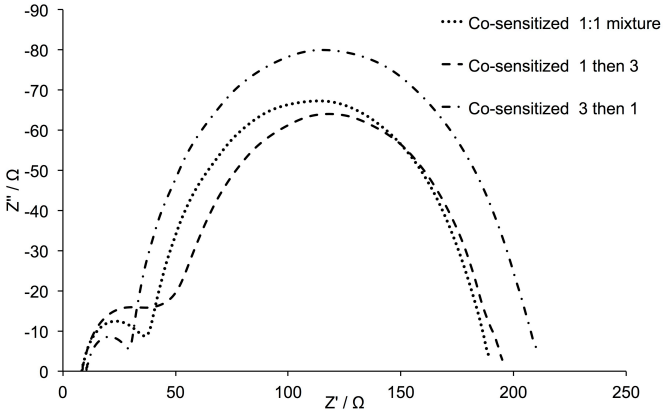

Fig 19. Nyquist plots of DSCs containing mixtures of the dyes $[Cu(\mathbf{5})(\mathbf{1})]^+$ and $[Cu(\mathbf{5})(\mathbf{3})]^+$ at a light intensity of 22 mW cm^{-2}. Three different dye-bath procedures were used (see text).

The comparison of EIS data for DSCs made with a combination of dyes versus a single dye shows the dominant effect of ancillary ligand **1** on the device performance. The data are consistent with the solid-state absorption measurements (Fig. 12) and the *J–V* measurements (Fig. 13) discussed above and indicate that ancillary ligand **1** replaces **3** more efficiently than *vice versa*. When a '**3** then **1**' dipping procedure is used, the EIS parameters are comparable to single-dye DSCs containing the surface-bound dye $[Cu(\mathbf{5})(\mathbf{1})]^+$. Both cells have the same R_{tr}, comparable R_{rec} and C_μ, as well as similar τ at a light intensity of 22 mW cm^{-2}. On the other hand, DSCs assembled by the '**1** then **3**' dipping method have a much lower C_μ than the single dye DSCs with single surface-bound dye $[Cu(\mathbf{5})(\mathbf{3})]^+$. Furthermore, R_{rec} is lower and R_{tr} is more than twice the value of the appropriate single dye DSC. Additionally, the electron lifetime τ at a light intensity of 22 mW cm^{-2} is only about the half of the single dye DSCs. This results in the lower overall efficiency of DSCs made using the '**1** then **3**' dipping procedure.

Conclusions

The synthesis and characterization of four new homoleptic copper(I) complexes $[Cu(\mathbf{1})_2][PF_6]$, $[Cu(\mathbf{2})_2][PF_6]$, $[Cu(\mathbf{3})_2][PF_6]$ and $[Cu(\mathbf{4})_2][PF_6]$ have been described, along with the single crystal structures of $[Cu(\mathbf{2})_2][PF_6]\cdot 0.5CH_2Cl_2$ and $[Cu(\mathbf{3})_2][PF_6]$. The latter confirms that the tetrahedral copper(I) centre is bound by *N,N'*-ligands. At 298 K, well-resolved solution ^1H NMR spectra are observed for $[Cu(\mathbf{2})_2][PF_6]$, $[Cu(\mathbf{3})_2][PF_6]$ and $[Cu(\mathbf{4})_2][PF_6]$, but for $[Cu(\mathbf{1})_2][PF_6]$ the signals are broad. Variable temperature NMR spectroscopic data are consistent with dynamic behaviour which we attribute to on–off coordination involving tautomers of the imidazole unit combined with rotation about the $C_{pyridine}$–$C_{imidazole}$ bond. The heteroatom has an influence on the energy of the MLCT band in the solution absorption spectrum, and the band shifts to lower energy in the order O < NH < NMe < S. In solution, $[Cu(\mathbf{1})_2][PF_6]$ and $[Cu(\mathbf{4})_2][PF_6]$ undergo copper-centred oxidative processes at lower potential than the complexes with O or S heteroatoms.

We have investigated the performances of duplicate, fully-masked DSCs containing the surface-bound heteroleptic dyes $[Cu(\mathbf{5})(L)]^+$ with L = **1**–**4**. The shift in the MLCT band (O ~ NH < NMe < S) in the solid-state absorption spectra of the dye-functionalized electrodes follows a similar trend to that observed in solution. The photoconversion efficiences of DSCs containing surface-assembled and surface-bound $[Cu(\mathbf{5})(L)]^+$ (L = **1**–**4**) dyes and an I^-/I_3^- redox couple follow the order $[Cu(\mathbf{5})(\mathbf{1})]^+$ (3.03%) > $[Cu(\mathbf{5})(\mathbf{3})]^+$ (2.88%) > $[Cu(\mathbf{5})(\mathbf{4})]^+$ (2.71%) > $[Cu(\mathbf{5})(\mathbf{2})]^+$ (2.62%) relative to 7.55% for N719. A significant observation is that use of ancillary ligand **1** (with NH) leads to the highest V_{OC} (608 mV) whilst **3** (S-heteroatom) gives the highest J_{SC} (7.76 mA cm^{-2}). EIS gives valuable insights into the reasons why $[Cu(\mathbf{5})(\mathbf{1})]^+$ and $[Cu(\mathbf{5})(\mathbf{3})]^+$ perform well. The DSC with $[Cu(\mathbf{5})(\mathbf{1})]^+$ exhibits a high C_μ and a low R_{rec}; since the latter is offset by a low R_{tr}, a high J_{SC} and V_{OC} are observed for $[Cu(\mathbf{5})(\mathbf{1})]^+$. DSCs with $[Cu(\mathbf{5})(\mathbf{3})]^+$ have the lowest R_{tr} of all four devices.

Co-sensitization of DSCs using combinations of copper(I) dyes has, to our knowledge, not previously been investigated. In this work we have assessed the performance of DSCs sensitized by a combination of $[Cu(\mathbf{5})(\mathbf{1})]^+$ and $[Cu(\mathbf{5})(\mathbf{3})]^+$, the aim being to exploit the high V_{OC} of $[Cu(\mathbf{5})(\mathbf{1})]^+$ and the high J_{SC} of $[Cu(\mathbf{5})(\mathbf{3})]^+$. We conclude that the order in which the anchoring ligand-functionalized FTO/TiO_2 electrodes are exposed to $[Cu(\mathbf{1})_2]^+$ and $[Cu(\mathbf{3})_2]^+$ has a significant impact of the DSC performances. Observed values of J_{SC} and V_{OC}, and EIS parameters are consistent with competition between **1** and **3** for surface binding-sites, with ancillary ligand **1** preferred over **3**, both in binding and in contribution to the overall photoresponse. DSCs made with FTO/TiO_2/**5** electrodes treated with a 1:1 mix of $[Cu(\mathbf{1})_2][PF_6]$ and $[Cu(\mathbf{3})_2][PF_6]$ or sequentially with $[Cu(\mathbf{3})_2][PF_6]$ then $[Cu(\mathbf{1})_2][PF_6]$ show similarly high J_{SC} values (7.20 and 6.91 mA cm^{-2}) and comparable V_{OC} (592 and 588 mV) leading to photoconversions of 3.02 and 2.96% relative to 7.55% for N719. However, sequential treatment with $[Cu(\mathbf{1})_2][PF_6]$ then $[Cu(\mathbf{3})_2][PF_6]$ is detrimental to DSC performance.

Overall, we conclude that when ancillary ligands **1** and **3**, although structurally simple, are combined in a surface-bound heteroleptic copper(I) dye with the phosphonic acid anchoring ligand **5**, photoconversion efficiencies reaching 40% that of the ruthenium dye N719 are achieved. This is the first report of co-sensitization of DSCs using combinations of copper(I) dyes. This is an important development as it opens the way to a strategy for harvesting the full solar energy spectrum without the need for designing new panchromatic complexes.

Acknowledgements

We acknowledge the Swiss National Science Foundation (Grant number 200020_162631), the Swiss Nano Institute (for the purchase of the EIS instrument) and the University of Basel for financial support.

Notes and references

[a]Department of Chemistry, University of Basel, Spitalstrasse 51, CH-4056 Basel, Switzerland; email: catherine.housecroft@unibas.ch

†Electronic Supplementary Information (ESI) available: See DOI: 10.1039/b000000x/

1 M. Grätzel, *Acc. Chem. Res.*, 2009, **42**, 1788; M. Grätzel, *Inorg. Chem.*, 2005, **44**, 6841; M. Grätzel, *J. Photochem. Photobiol. C*, 2003, **4**, 145 and references therein..

2 K. Kalyanasundaram, ed., *Dye Sensitized Solar Cells*, 2010, CRC Press, Boca Raton.

3 B. O'Regan and M. Grätzel, *Nature*, 1991, **353**, 737.

4 A. Mishra, M. Fischer and P. Bäuerle, *Angew. Chem. Int. Ed.*, 2009, **48**, 2474.

5 A. Yella, H.-W. Lee, H. N. Tsao, C. Yi, A. K. Chandiran, M. K. Nazeeruddin, E. W.-G. Diau, C.-Y. Yeh, S. M. Zakeeruddin and M. Grätzel, *Science*, 2011, **334**, 629.

6 T. Higashino and H. Imahori, *Dalton Trans*., 2015, **44**, 448.

7 A. Hagfeldt and M. Grätzel, *Acc. Chem. Res.*, 2000, *33*, 269.

8 A. Hagfeldt, G. Boschloo, L. Sun, L. Kloo and H. Pettersson, *Chem. Rev*., 2010, **110**, 6595.

9 Y. Xie, Y. Tang, W. Wu, Y. Wang, J. Liu, X. Li, H. Tian and W.-H. Zhu, *J. Am. Chem. Soc*., 2015, **137**, 14055.

10 H. Ozawa, Y. Okuyama and H. Arakawa, *ChemPhysChem*, 2014, **15**, 1201.

11 K. Kakiage, Y. Aoyama, T. Yano, T. Otsuka, T. Kyomen, M. Unno and M. Hanaya, *Chem. Commun*., 2014, **50**, 6379.

12 C.-Y. Chen, M. Wang, J.-Y. Li, N. Pootrakulchote, L. Alibabaei, C-ha Ngoc-le, J.-D. Decoppet, J.-H. Tsai, C. Grätzel, C.-G. Wu, S. M. Zakeeruddin and M. Grätzel, *ACS Nano*, 2009, **3**, 3103.

13 S. Mathew, A. Yella, P. Gao, R. Humphry-Baker, B. F. E. Curchod, N. Ashari-Astani, I. Tavernelli, U. Rothlisberger, Md. K. Nazeeruddin and M. Grätzel, *Nature Chem*., 2014, **6**, 242.

14 K. Kakiage, Y. Aoyama, T. Yano, K. Oya, T. Kyomen and M. Hanaya, *Chem. Commun*., 2015, **51**, 6315.

15 Z. Yao, M. Zhang, H. Wu, L. Yang, R. Li and P. Wang, *J. Am. Chem. Soc.*, 2015, **137**, 3799.

16 K. Kakiage, Y. Aoyama, T. Yano, K. Oya, J-i. Fujisawa and M. Hanaya, *Chem. Commun.*, 2015, **51**, 15894.

17 See for example: E. Singh and H.S. Nalwa, *Science Adv. Mater.*, 2015, **7**, 1863; S. Thomas, T.G. Deepak, G.S. Anjusree, T.A. Arun, S.V. Nair and A.S. Nair, *J. Mater. Chem. A*, 2014, **2**, 4474; M. Wang, J. Ioccozia, L. Sun, C. Lin and Z. Lin, *Energy Environ. Sci.*, 2014, **7**, 2182; M. Ye, D. Zheng, M. Lv, C. Chen, C. Lin and Z. Lin, *Adv. Mater*., 2013, **25**, 3039; Y.H. Jang, X. Xin, M. Byun, Y.J. Jang, Z. Lin and D.H. Kim, Nano Lett., 2012, **12**, 479; X. Meng, C. Yu, X. Song, Y. Liu, S. Liang, Z. Liu, C. Hao and J. Qiu, *Adv. Energy Mater*., 2015, 1500180; X. Meng, C. Yu, B. Lu, J. Yang and J. Qiu, *Nano Energy*, 2016, **22**, 59; C. Yu, X. Meng, X. Song, S. Liang, Q. Dong, G. Wang, C. Hao, X. Yang, T. Ma, P.M. Ajayan and J. Qiu, *Carbon*, 2016, **100**, 474.

18 Y. Xu, L.-S. Qiang, Y.-L. Yang, L.-G. Wei, P. Wang and R.-Q. Fan, *Chinese Chem. Lett.*, 2016, **27**, 127.

19 See for example: Y. Ogomi, S. S. Pandey, S. Kimura and S. Hayase, *Thin Solid Films*, 2010, **519**, 1087; G. Koyyada, S. Shome, M. Chandrasekharam, G. D. Sharma and S. P. Singh, *RSC Adv*., 2016, **6**, 41151; D. D. Babu, R. Su, A. El-Shafei and A. V. Adhikari, *RSC. Adv*., 2016, **6**, 30205; D. D. Babu, R. Su, A. El-Shafei and A. V. Adhikari, *Electrochimica Acta*, 2016, **198**, 10; D. D. Babu, D. Elsherbiny, H. Cheema, A. El-Shafei and A. V. Adhikari, *Dyes and Pigments*, 2016, **132**, 316; U. Mehmood, I. A. Hussein, K. Harrabi, N. Tabete and G. R. Berdiyorov, *RSC Adv*., 2016, **6**, 7897; L. Wei, Y. Yang, Z. Zhu, R. Fan, P. Wang, Y. Dong and S. Chen, *RSC Adv*., 2015, **5**, 96934; L. Wei, Y. Yang, R. Fan, Y. Na, P. Wang and Y. Dong, *Thin Solid Films*, 2015, **592**, 14; P. Salvatori, S. Agrawal, C. Barreddi, C. Malapaka, M. de Borniol and F. De Angelis, *RSC Adv*., 2014, **4**, 57620; L. Wei, Y. Na, Y. Yang, R. Fan, P. Wang and L. Li, *Phys. Chem. Chem. Phys*., 2015, **17**, 1273; J. Luo, Z. Wan, C. Jia, Y. Wang, X. Wu and X. Yao, *Electrochimica Acta*, 2016, **211**, 364;

20 B.E. Hardin, A. Sellinger, T. Moehl, R. Humphry-Baker, J.-E. Moser, P. Wang, S.M. Zakeeruddin, M. Grätzel and M.D. McGehee, *J. Am. Chem. Soc.*, 2011, **133**, 10662.

21 L.H. Nguyen, H.K. Mulmudi, D. Sabba, S.A. Kulkarni, S.K. Batabyal, K. Nonomura, M. Grätzel and S.G. Mhaisalkar, *Phys. Chem. Chem. Phys.*, 2012, **14**, 16182.

22 G.D. Sharma, P.A. Angaridis, S. Pipou, G.E. Zervaki, V. Nikolaou, R. Misra and A.G. Coutsolelos, *Org. Electronics*, 2015, **25**, 295.

23 S. Fan, X. Lu, H. Sun, G. Zhou, Y. J. Chang and Z.-S. Wang, *Phys. Chem. Chem. Phys*., 2016, **8**, 932.

24 A. Yella, H.-W. Lee, H.N. Tsao, C. Yi, A.K. Chandiran, Md.K. Nazeeruddin, E.W.-G. Diau, C.Y. Yeh, S.M. Zakeeruddin, M. Grätzel, *Science*, 2011, **334**, 629.

25 J.-J. Cid, J.-H. Yum, S.-R. Jang, M.K. Nazeeruddin, E. Martínez-Ferrero, E. Palomares, J. Ko, M. Grätzel and T. Torres, *Angew. Chem. Int. Ed.*, 2007, **46**, 8358.

26 See for example: H. Li, Y. Wu, Z. Geng, J. Liu, D. Xua and W. Zhu, *J. Mater. Chem. A*, 2014, **2**, 14649; C. Magne, M. Urien and T. Pauporté, *RSC Adv*., 2013, **3**, 6315; T. H. Nguyen, T. Suresh and J. H. Kim, *Organic Electronics*, 2016, **30**, 40; K. Kakiage, Y. Aoyama, T. Yano, K. Oya, T. Kyomenb and M. Hanaya, *Chem. Commun*., 2015, **51**, 6315; M. Fang, H. Li, Q. Li and Z. Li, *RSC Adv*., 2016, **6**, 40750; A. Islam, Md. Akhtaruzzaman, T. H. Chowdhury, C. Qin, L. Han, I. M. Bedja, R. Stalder, K. S. Schanze and J. R. Reynolds, *ACS*

Appl. Mater. Interfaces, 2016, **8**, 4616; X. Lu, T. Lan, Z. Qin, Z.-S. Wang and G. Zhou, *ACS Appl. Mater. Interfaces*, 2014, **6**, 19308;

27 C. S. K. Ranasinghe, W. M. N. M. B. Wanninnayake, G. R. A. Kumara, R. M. G. Rajapakshe and P. M. Sirimanne, *Optik*, 2014, **125**, 813.

28 C. E. Housecroft and E. C. Constable, *Chem. Soc. Rev.*, 2015, **44**, 8386 and references therein.

29 M. Magni, P. Biagini, A. Colombo, C. Dragonetti, D. Roberto and A. Valore, *Coord. Chem. Rev*., 2016, **322**, 69 and references therein.

30 M. Sandroni, Y. Pellegrin and F. Odobel, *C. R. Chimie*, 2016, **19**, 79 and references therein.

31 F. J. Malzner, S. Y. Brauchli, E. C. Constable, C. E. Housecroft and M. Neuburger, *RSC Adv.*, 2014, **4**, 48712.

32 F. Brunner, M. Klein, S. Keller, C. D. Morris, A. Prescimone, E. C. Constable and C. E. Housecroft, *RSC Adv.*, 2015, **5**, 58694.

33 C.T. Cunningham, J.J. Moore, K.L.H. Cunningham, P.E. Fanwick and D.R. McMillin, *Inorg. Chem.*, 2000, **39**, 3638.

34 H.-Q. Do, R.M.K. Khan and O. Daugulis, *J. Am. Chem. Soc*., 2008, **130**, 15185.

35 F. Derridj, J. Roger, F. Geneste, S. Djebbar and H. Doucet, *J. Organomet. Chem.*, 2009, **694**, 455.

36 R. Gao, L. Xiao, X. Hao, W.-H. Sun and F. Wang, *Dalton. Trans.*, 2008, 5645.

37 C. Rai and J.B. Braunwarth, *J. Org. Chem*., 1961, **26**, 3434.

38 M.J. Saif and K.R. Flower, *Transition Met. Chem.*, 2013, **38**, 113.

39 W.-H. Sun, P. Hao, S. Zhang, Q. Shi, W. Zuo, X. Tang and X. Lu, *Organometallics,* 2007, **26**, 2720.

40 G.J. Kubas, *Inorg. Synth*., 1990, **28**, 68.

41 Bruker Analytical X-ray Systems, Inc., 2006, APEX2, version 2 User Manual, M86-E01078, Madison, WI.

42 L. Palatinus and G. Chapuis, *J. Appl. Cryst*., 2007, **40**, 786.

43 P. W. Betteridge, J. R. Carruthers, R. I. Cooper, K. Prout and D. J. Watkin, *J. Appl. Cryst*., 2003, **36**, 1487.

44 A. L. Spek, *Acta Crystallogr., Sect. D* 2009, 65, 148.

45 I. J. Bruno, J. C. Cole, P. R. Edgington, M. K. Kessler, C. F. Macrae, P. McCabe, J. Pearson and R. Taylor, *Acta Cryst. B*, 2002, **58**, 389.

46 C. F. Macrae, I. J. Bruno, J. A. Chisholm, P. R. Edgington, P. McCabe, E. Pidcock, L. Rodriguez-Monge, R. Taylor, J. van de Streek and P. A. Wood, *J. Appl. Cryst*., 2008, **41**, 466.

47 H. J. Snaith, *Energy Environ. Sci.*, 2012, **5**, 6513.

48 H. J. Snaith, *Nature Photonics*, 2012, **6**, 337.

49 M. Nishio, *CrystEngComm*, 2004, **6**, 130.

50 B. Bozic-Weber, V. Chaurin, E. C. Constable, C. E. Housecroft, M. Meuwly, M. Neuburger, J. A. Rudd, E. Schönhofer and L. Siegfried, *Dalton Trans*., 2012, **41**, 14157.

51 A. Begum and P.G. Pickup, *Electrochem. Comm.*, 2007, **9**, 2525.

52 B. Bozic-Weber, V. Chaurin, E. C. Constable, C. E. Housecroft, M. Meuwly, M. Neuburger, J. A. Rudd, E. Schönhofer and L. Siegfried *Dalton Trans*., 2012, **41**, 14157

53 B. Wenger, M. Grätzel and J.-E. Moser, *J. Am. Chem. Soc.*, 2005, **127**, 12150.

54 B. Wenger, M. Grätzel and J.-E. Moser, *Chimia*, 2005, **59**, 123.

55 V. K. Thorsmølle, B. Wenger, J.Teuscher, C. Bauer and J.-E. Moser, *Chimia*, 2007, **61**, 631.

56 F. J. Malzner, S. Y. Brauchli, E. Schönhofer, E. C. Constable and C. E. Housecroft, *Polyhedron*, 2014, **82**, 116.

57 Md. K. Nazeeruddin, S. M. Zakeeruddin, R. Humphry-Baker, M. Jirousek, P. Liska, N. Vlachopoulos, V. Shklover, C.-H. Fischer and M. Grätzel, *Inorg. Chem.*, 1999, **38**, 6298.

58 S.G. Yan and J.T. Hupp, *J. Phys. Chem.*, 1996, **100**, 6867.

59 D.D. Macdonald, *Electrochimica Acta*, 2006, **51**, 1376.

60 B.-Y. Chang and S.-M. Park, *Annu. Rev. Anal. Chem.*, 2010, **3**, 207.

61 F. Fabregat-Santiago, G. Garcia-Belmonte, I. Mora-Seró and J. Bisquert, *Phys. Chem. Chem. Phys*., 2011, **13**, 9083.

62 J. Bisquert, *J. Electroanal. Chem.*, 2010, **646**, 43.

63 F. Fabregat-Santiago, J. Bisquert, E. Palomares, L. Otero, D. Kuang, S. M. Zakeeruddin and M. Grätzel, *J. Phys. Chem. C*, 2007, **111**, 6550.

64 Q. Wang, J.-E. Moser and M. Grätzel, *J. Phys. Chem. B*, 2005, **109**, 14945.

65 Y. Baumgartner, Y. M. Klein, E. C. Constable, C. E. Housecroft and M. Willgert, *RSC Adv*., 2016, **6**, 86220.

66 Q. Wang, S. Ito, M. Grätzel, F. Fabregat-Santiago, I. Mora-Seró, J. Bisquert, T. Bessho and H. Imai, *J. Phys. Chem. B,* 2006**, 110***,* 25210.

67 M. Liberatore, F. Decker, L. Burtone, V. Zardetto, T.M. Brown, A. Reale and A. Di Carlo, *J. Appl. Electrochem.*, 2009, **39**, 2291.

68 Y. Liu, A. Hagfeldt, X.-R. Xiao and S.-E. Lindquist, *Sol. Energy Mater. Sol. Cells*, 1998, **55**, 267.